# Shear resistance of perforated QN1803 high-strength stainless steel plate girders through experimental testing and numerical analysis

Boshan Chen[a], Yuanqing Wang[a], Jun Ye[b], James B.P. Lim [c,d], Letian Hai[a*]

[a] Department of Civil Engineering, Tsinghua University, P.R China

[b] School of civil engineering, University of Leeds, United Kingdom

[c] School of Engineering, The University of Waikato, New Zealand

[d] Department of Civil and Environmental Engineering, The University of Auckland, New Zealand

**Abstract:** QN1803, a high-strength stainless steel, has been developed by steel industry recently. Its tensile yield strength can be approximately 40% (or more) higher than that of the commonly-used EN1.4301, while its cost is 20% lower due to its reduced nickel content. One obvious application for QN1803 is in plate girders, where web perforations are often required to accommodate building services. However, no research work has been reported in the literature that investigates the reduced shear buckling capacity of QN1803 plate girders as a result of web perforations. This issue is addressed herein. An experimental program comprising six plate girder tests is conducted in this study. Three different hole ratios were considered: 0.2, 0.4 and 0.6. The depths of web were selected as 700 mm and 500 mm, while the thickness of web was fixed as 4.0mm. The initial geometric imperfections were determined from three-dimensional (3D) scanning prior to the plate girder tests. Finite element (FE) models incorporating the material non-linearity and initial geometric imperfections were then developed and validated against the experimental results. A parametric analysis including 62 FE models was performed to examine the influences of the critical parameters on the shear buckling capacity of such perforated members. The results suggest that for those members with a hole diameter - web height ratio of 0.6, the shear buckling capacity was reduced by 56% on average due to the web perforation. The design rules for determining the shear buckling

capacity of stainless steel plate girders as specified in Eurocodes (EN 1993-1-4+A1) (2015) and American Specification (ANSI/AISC 370-21) (2021) were evaluated. Upon comparison, it was demonstrated that both EN 1993-1-4+A1 (2015) and ANSI/AISC 370-21 (2021) cannot provide accurate and safe predictions for determining the shear buckling capacity of such members.

**Keywords:** QN1803 stainless steel, plate girder tests, web perforations, shear buckling capacity, experimental testing, numerical analysis

# 1. Introduction

QN1803 (also known as 304D), a high-strength stainless steel, has been developed by steel industry recently [1]. It is the first austenitic stainless steel containing nitrogen, and such new material can offer higher corrosion resistance, reduced cost (estimated at 20%), and higher yield strength (estimated at 40%), when compared with the commonly-used stainless steel EN 1.4301. This high-performance material can potentially be used in various applications, one of which is in plate girders. Plate girders often require web perforations to accommodate building services (see Fig. 1). Such web perforations, however, can lead to a reduction in the shear buckling capacity.

In the literature, extensive research has been conducted on the shear buckling capacity of normal-strength stainless steel plate girders with unperforated webs. Examples of such research include the works of Real et al. [2], Estrada et al. [3-4], Saliba et al. [5-6] and Chen et al. [7]. They found that the shear buckling capacity of normal-strength stainless steel plate girders differs from that of carbon steel plate girders due to differences in material characteristics and residual stress. Also, the existing design approaches for carbon steel were found to be inappropriate for normal-strength stainless steel plate girders. It should be noted that all the above-mentioned research was conducted on unperforated members i.e. web perforations were not considered.

In terms of normal-strength stainless steel plate girders with perforated webs, only Chen et al. [8-9] investigated the shear buckling behaviour of normal-strength stainless steel plate girders with perforated webs. A total of eight plate girders made of austenitic EN 1.4301 and duplex EN 1.4462 stainless steel were tested. The comparison indicated that the current design rules were not appropriate for calculating the shear buckling capacity of such plate girders with perforated webs. However, it should be noted that both EN 1.4301 and EN 1.4462 stainless steel investigated by Chen et al. [8-9] differ from QN1803 in terms of material properties.

Regarding high-strength stainless steel plate girders, limited work is available in the literature. Xue et al. [10] conducted a comprehensive numerical investigation to determine the shear buckling capacity of S600E high-strength stainless steel plate girders; S600E represents a new generation of sorbite stainless steel with higher yield strength. Only Chen et al. [11-12] have numerically and experimentally investigated the shear buckling capacity of QN1803 plate girders. A total of seven plate girder tests were conducted, indicating that the shear buckling capacity of QN1803 plate girders increased by 38.2% on average, compared to EN 1.4301 plate girders. However, these plate girder tests were conducted on those unperforated members.

This study presents a detailed experimental program including six plate girder tests to determine the shear buckling capacity of high-strength stainless steel plate girders with perforated webs. The plates are made of austenitic grade QN1803. The distribution of initial geometric imperfections was determined from three-dimensional (3D) scanning prior to shear tests. Finite element (FE) models incorporating the material non-linearity and initial geometric imperfections were then developed. The results of FE models were compared against the experimental results, which were further employed to undertake a parametric analysis. To evaluate the impact of various factors on the shear buckling capacity, the web aspect ratios, end-post conditions, web slenderness and hole ratios were investigated in the parametric analysis. The currently available design approaches as specified in the Eurocodes (EN 1993-1-4+A1) [13] and American specification (ANSI/AISC 370-21) [14] were evaluated using the experimental and numerical results.

## 2. Experimental testing

*2.1 Details of test specimens*

A total of six plate girders were examined, as shown in Fig. 2(a), in which five specimens were designed to contain free-end posts (Fig. 2(b)), while the remaining one contained strengthened-end posts (Fig. 2(c)), as illustrated in Table 1. All tested specimens were made of QN1803, which has been developed recently. The measured dimensions of each specimen are summarized in Table 1, in which $L$ is the total length of specimen, $a$ is the length of web, $h_w$ is the height of web, $t_w$ is the thickness of the web, $d_{wh}$ is the diameter of web perforation, and $w_0$ is the measured maximum value of initial geometric imperfections generated from the three-dimensional (3D) scanner. Fig. 2 displays the geometry of test specimens used in this study.

The objective of this research work is to evaluate the effect of web perforation on the shear buckling capacity of such plate girders, which is governed by shear failure. As a result, the test specimens were designed to have a large depth and short span to minimize the effect of combined bending and shear loading. The depths of web ($h_w$) were selected as 700 mm and 500 mm. All web sections were classified as Class 4 with respect to bending as per EN 1993-1-4+A1 [13]. Two aspect ratios ($\beta$=$a$/$h_w$) were considered: 1.0 and 1.5. In the case of perforated specimens, the perforations were manufactured in the mid-height of web using the laser cutting technique. Three different hole ratios ($d_{wh}$/$h_w$) were considered: 0.2, 0.4 and 0.6. For comparison, test results of specimens with unperforated webs, as reported by Chen et al. [12], have also been summarized in Table 1. The flange of the plate girders ($t_f$) was designed to have a nominal thickness of 12mm, while the nominal thickness of the web ($t_w$) was fixed as 4.0mm. Both cases of strengthened-end posts and free-end posts were examined. It should be noted that for those specimens featuring strengthened-end posts, the strengthened-end post conditions were achieved using a pair of transverse stiffeners at two ends [15].

A labelling system is employed to indicate the specimens, providing information regarding stainless steel grade, web depth, aspect ratio, hole ratio, and end conditions. For example, the labelling “V304D-H500-ad1.0-A0.6-R” may be interpreted as follows: “304D” means that the grade of stainless steel is 304D (QN1803); “500” indicates that the height of web ($h_w$) is 500 mm; “ad1.0” indicates that the aspect ratio ($a/h_w$) is 1.0; “A0.6” indicates that the hole diameter to web height ratio ($d_{wh}/h_w$) is 0.6; “R” means specimen featuring strengthened-end posts.

*2.2 Material characteristics*

To examine the non-linear characteristics of stainless steel material, a 300 kN testing machine was used to conduct a total of six tensile coupon experiments following the guidelines outlined in ISO 6892-1 [16], as illustrated in Fig. 3(a). The samples were obtained from the untested specimens, oriented parallel to the rolling direction (longitudinal direction). Three identical coupons were manufactured for each thickness. The measured thickness of the tensile coupons reported in Table 2 was determined based on the parameters “$t_w$”, and a vernier caliper was used for measurement. The full stress versus strain curves obtained from QN1803 are depicted in Fig. 3(b). The test data generated from the tensile experiments are presented in Table 2, which could be used for the development of numerical models. It should be noted that the plate girder tests were performed on the same batch of those specimens with unperforated webs, which was investigated by the authors previously [12]. Therefore, the material properties of the test specimens examined in this study are the same as those reported by Chen et al. [12].

*2.3. Measuring geometric imperfections*

As a consequence of the manufacturing, transportation, and handling procedures, the majority of steel members have initial geometric imperfections. The influence of these geometric imperfections on the shear characteristics of stainless steel plate girders cannot be ignored. Consequently, the initial values of their local geometric imperfections were accurately determined from a 3D laser scanner prior to the shear testing.

As illustrated in Fig.4, a portable 3D laser scanner (FreeScan X7) with an accuracy rate of 0.02 mm was utilized. The FreeScan X7 is capable of achieving a scanning speed of 480,000 points per second. The initial step involved creating a 3D point-cloud model using the handheld 3D laser scanner, and subsequently, a computer program (3D Pr.) based on data processing algorithms was developed to transform the 3D point-cloud model into an accurate digital geometric model. This allowed for the extraction of both global and local initial geometric imperfections, with the maximum values of local geometric imperfections being automatically derived. The procedures and equipment for measuring geometric imperfections in this study were also reported by Xu et al. [17]. The maximum values of local geometric imperfections generated from the 3D scanning technique ($w_0$) are summarized in Table 1. The distributions of measured geometric imperfections are depicted in Fig.5.

*2.4 Testing setup and loading process*

Fig. 6 displays a photograph and schematic diagram of the experimental setup, which has been used by other studies [2-7]. The shear tests were conducted using the MTS hydraulic machine with a 2000 kN capacity. The test specimens were supported by means of two bearings at both ends. A concentrated loading at the mid-span was applied using a rigid bearing block with a width of 160 mm, and it should be noted that the effect of the width of the bearing block on the ultimate strength could be negligible. Two clamped supports were used at both ends of the test specimens to limit their out-of-plane displacements. It should be mentioned that during the testing process, a small clearance was maintained between the test specimen and the clamped supports. Moreover, lubricating oil was used to reduce possible friction. To obtain the vertical displacement at both ends and the mid-span, three displacement transducers (LVDTs) were employed, as shown in Fig. 6.

*2.5 Test results and discussion*

The failure mechanism of specimens V304D-H500-ad1.0-A0.2, V304D-H500-ad1.0-A0.4 and V304D-H500-ad1.0-A0.6 is illustrated in Figs. 7-9, respectively. It can be observed that shear buckling failure occurred at the web for all test specimens. Moreover, the tension bands developed in the web and the plastic hinge formed at the flanges. Also, the local buckling phenomenon occurred at both ends for those specimens containing free-end posts, distinguishing them from specimens containing strengthened-end posts.

Table 1 presents a summary of the key experimental results obtained from the shear tests, where $V_{\mathrm{u,test}}$ is the shear buckling capacity generated from the experiments. It was found that the shear buckling capacity of those specimens featuring strengthened-end posts increased, which can be attributed to the presence of stiffeners at both ends.

Fig.10 illustrates the ultimate capacity plotted against the mid-span vertical displacement of all test specimens, in which most of those curves were horizontally stabilized after reaching the ultimate strength. It can be found that all of test specimens experienced a significant level of ductility prior to shear failure.

The impact of web perforation on ultimate strength was studied, as shown in Fig. 11. The results suggested that the shear buckling capacity experienced a significant reduction due to the impact of web perforations, which was directly proportional to the hole ratio ($d_{\mathrm{w}}/h_{\mathrm{w}}$). For those members containing a hole ratio of 0.6, the shear buckling capacity was reduced by 56% on average, compared to that of those members containing unperforated webs.

The impact of aspect ratio on the strength of perforated high-strength stainless steel members was also investigated. It was found that for those members containing an aspect ratio of 1.5, a decrease of 18.3% in shear buckling capacity was observed, compared to that of members containing an aspect ratio of 1.0.

## 3. Numerical analysis

### *3.1 General*

A numerical analysis was performed using ABAQUS software [18] to assess the shear buckling capacity of QN1803 high-strength stainless steel plate girders with perforated webs. FE models were developed to incorporate material nonlinearity and initial geometric imperfections, and their accuracy was validated by comparing them to the corresponding test results. Similar modelling approaches have been employed by the authors in previous studies [19-21]. Further information can be found in the work of Chen et al. [8].

### *3.2 Modelling of material properties*

The material properties of test specimens were simulated using von Mises material model with isotropic hardening. The stress-strain curve obtained from tensile coupon tests were used in the numerical analysis, and these curves were subsequently incorporated into the models using the two-stage modified Ramberg-Osgood equations proposed by Gardner and Ashraf [22]. To include the nonlinear material properties of QN1803, the engineering material data were transformed into actual material data using the following equations: (1)-(2):

$$\sigma_{true} = \sigma(1+\varepsilon) \tag{1}$$

$$\varepsilon_{true(pl)} = \ln(1+\varepsilon) - \frac{\sigma_{true}}{E} \tag{2}$$

*3.3 Finite element type and meshing*

To simulate the high-strength stainless steel plate girders, a four-node shell element (S4R) was employed, as its thickness was significantly smaller compared to the other dimensions. A study on mesh sensitivity was conducted, varying the mesh size from 2 mm to 50 mm. The effects of different mesh element sizes on the ultimate strength of these girders were assessed, leading to the selection of a 10 mm × 10 mm mesh size. A finer mesh size around the web perforations was defined for obtaining accurate results [19], and a mesh size of 5 mm × 5 mm was used. The specific mesh size utilized in the FE models is depicted in Fig. 12(a).

*3.4 Boundary and loading conditions*

The FE models developed in this investigation employed the same loading arrangement as the laboratory tests. To apply concentrated loading at the mid-span, a vertical displacement was defined at a reference point, and this reference point was connected to the upper surface of the flange. A TIE constraint was used to simulate the welding connection between the web, flange, and stiffener (see Fig. 12(b)). To simulate the strengthened-end posts, two reinforced plates were constructed at each end. The TIE constraint was utilized to simulate the interconnection between the end surfaces and the reinforced plates in the FE models. However, no reinforced plates were incorporated for plate girders containing free-end posts.

*3.5 Modelling of initial geometric imperfections and residual stresses*

In terms of the initial geometric imperfections, an elastic buckling analysis was initially conducted to determine the initial buckling mode (Fig. 12(c)) [20]. The lowest mode shape obtained from the elastic buckling analysis was in a good agreement with the initial geometric imperfections observed in the tests. Therefore, the impact of geometric imperfections was incorporated into the FE models using the *IMPERFECTION keyword, based on the initial buckling mode and the measured value of $w_0$ provided in Table 1.

The influence of residual stress on the shear buckling capacity of these high-strength stainless steel plate girders was found to be negligible, with an effect of less than 1% [8-9]. Consequently, the FE models developed in this study did not account for the impact of residual stress. The structural behaviour of these plate girders was evaluated using the RIKS approach, and a nonlinear key parameter (*NLGEOM) was employed in the FE models.

*3.6 Validation of numerical model*

The validation results of the constitutive model used in this numerical analysis were reported by the authors previously [12]. A comparison between the modified R-O model [13] and test results was performed, indicating that both constitutive models could closely predict the tensile behaviour of such QN1803 high strength stainless steel. More details regarding the validation results could be found in Chen et al. [12].

The results obtained from six experiments were utilized to validate the accuracy of the FE models. The shear buckling capacity generated from the laboratory tests ($V_{\mathrm{u,\,Test}}$) and numerical investigation ($V_{\mathrm{u,\,FEA}}$) were compared, as depicted in Table 1. The mean ratio of $V_{\mathrm{u,Test}}/V_{\mathrm{u,FEA}}$ was 0.98, with a coefficient of variation (COV) of 0.01. Moreover, Fig. 13 presents a comparison between the load-vertical displacement relationships obtained from laboratory tests and numerical simulations. It was found that most of two curves have a good agreement in terms of the initial stage and ultimate strength. Fig. 14 illustrates the failure mechanisms determined from laboratory tests and numerical investigations. It can be noted that the simulation results are in a good agreement with the experimental results regarding the failure mechanisms.

Therefore, the FE models established in this study demonstrated their ability to closely predict the shear behaviour of such QN1803 members in terms of shear buckling capacity and failure modes, which can be extended for further parametric analysis.

*3.7 Parametric analysis*

After successfully verifying the accuracy of the FE models, a parametric analysis was conducted, involving a total of 62 FE models. The primary objective of this investigation was to generate an extensive database for perforated high-strength stainless steel members undergoing shear forces. To evaluate the impact of various factors on the shear buckling capacity, the web aspect ratios, end-post conditions, web slenderness and hole ratios were investigated. Five different hole ratios ($d_{wh}/h_w$) were examined, namely 0.1, 0.5, 0.6, 0.7 and 0.8; The height-to-thickness ratio ($h_w/t_w$) was examined from 50 to 500; The web aspect ratio ($a/h_w$) varied from 0.50 to 1.50. Both cases of specimens containing strengthened-end posts and free-end posts were considered. The ranges of key parameters employed in this study are presented in Table 3.

Fig. 15 presents the effect of hole ratio on the shear buckling behaviour of such perforated high-strength stainless steel members. It was found that for specimens containing a hole ratio of 0.8, the presence of web perforations led to a reduction of 72.2% on average in shear buckling capacity, compared to specimens containing a hole ratio of 0.1. Fig. 16 illustrates how the shear buckling capacity and failure mode of perforated high-strength stainless steel members are affected by the aspect ratio ($a/h_w$), indicating that the value of shear buckling factor decreased significantly, when the aspect ratio ($a/h_w$) increased from 0.75 to 1.5. The impact of different end posts on the strength and behaviour of perforated high-strength stainless steel members was investigated, as depicted in Fig.17. The results indicated that for those members containing strengthened-end posts, an increase of 10% in shear buckling capacity was observed, compared to those containing free-end posts.

# 4. Summary of current design approaches

*4.1 General*

To evaluate the current design approaches for stainless steel plate girders, the design equations for stainless steel members with unperforated webs, as presented in EN 1993-1-4+A1 [13] and ANSI/AISC 370-21 [14], are summarised in this section, as no any design rules are available for QN1803 high-strength stainless steel plate girders with perforated webs.

*4.2 Design principles as outlined in EN 1993-1-4+A1 [13]*

The existing design approaches as specified in EN 1993-1-4+A1 [13] were developed for computing the shear buckling capacity of normal-strength stainless steel plate girders containing unperforated webs. The formulas that considered both strengthened-end and free-end posts were similar to those in EN 1993-1-5 [15]. As described by Saliba et al. [5-6], this approach developed for carbon steel was applied to normal-strength stainless steel members. Eq. (3) shows the expressions for computing shear buckling capacity provided by the webs ($V_{\mathrm{bw}}$), while Eqs. (4) and (5) show the expressions for computing the shear buckling factor ($\chi_{\mathrm{w}}$).

$$V_{bw} = \chi_w h_w t_w \frac{f_{yw}}{\sqrt{3}} \tag{3}$$

In terms of those specimens containing strengthened-end posts

$$\chi_w = \begin{cases} \eta & \left(\lambda_w \le \dfrac{0.65}{\eta}\right) \\ \dfrac{0.65}{\lambda_w} & \left(\dfrac{0.65}{\eta} < \lambda_w \le 0.65\right) \\ \dfrac{1.56}{(0.91+\lambda_w)} & \left(\lambda_w > 0.65\right) \end{cases} \tag{4}$$

In terms of those specimens containing free-end posts

$$\chi_{\mathrm{w}} = \begin{cases} \eta & \left(\lambda_{\mathrm{w}} \leq \dfrac{0.65}{\eta}\right) \\ \dfrac{0.65}{\lambda_{\mathrm{w}}} & \left(\dfrac{0.65}{\eta} < \lambda_{\mathrm{w}} \leq 0.65\right) \\ \dfrac{1.19}{\left(0.54 + \lambda_{\mathrm{w}}\right)} & \left(\lambda_{\mathrm{w}} > 0.65\right) \end{cases} \tag{5}$$

In which the calculation of the web slenderness ($\lambda_{\mathrm{w}}$) is performed using Eq. (6).

$$\lambda_w = \frac{h_w / t_w}{37.4\varepsilon_k \sqrt{\kappa_\tau}} \tag{6}$$

In which the shear buckling factor $\chi_{\mathrm{w}}$ could be calculated following the guidelines outlined in EN 1993-1-4+A1 [13]; $h_{\mathrm{w}}$ is the height of web; $t_{\mathrm{w}}$ is the thickness of web; $f_{\mathrm{yw}}$ is the yield strength of web; the factor $\eta$ is equal to 1.2.

*4.3 Design principles as outlined in ANSI/AISC 370-21 [14]*

In terms of design procedures as specified in ANSI/AISC 370-21 [14], the post-buckling strength without tension field action was employed, which was suitable for plate girders containing transverse stiffeners in shear. However, the design methods did not incorporate the influence of end conditions in ANSI/AISC 370-21 [14]. Furthermore, the expressions for computing the strength reduction factor ($C_{\mathrm{v1}}$) in ANSI/AISC 370-21 [14] were modified based on the experimental results reported by Chen et al. [7]. This modification was necessary because the performance of stainless steel is different from that of carbon steel in terms of material nonlinearity and strain-hardening behaviour.

The expression for ultimate strength ($V_{\mathrm{n1}}$) is given in Eq. (7), and the shear post-buckling strength factor ($C_{\mathrm{v1}}$) is calculated by Eq. (8).

$$V_{n1} = 0.6 F_y h_{\mathrm{w}} t_w C_{v1} \tag{7}$$

$$C_{\mathrm{v1}} = \begin{cases} 1.2 & h_{\mathrm{w}}/t_{\mathrm{w}} \leq 0.59\sqrt{k_v E / F_y} \\ \dfrac{1.55\sqrt{k_v E / F_y}}{0.7\sqrt{k_v E / F_y} + h_{\mathrm{w}}/t_{\mathrm{w}}} & h_{\mathrm{w}}/t_{\mathrm{w}} > 0.59\sqrt{k_v E / F_y} \end{cases} \tag{8}$$

## 5. Evaluation of design approaches using test and numerical results

*5.1. General*

To evaluate the accuracy of the existing design approaches, a total of 68 results including 6 testing and 62 numerical data were used. Table 4 provides a summary of the ultimate strength obtained from testing and parametric analysis, which were compared against the design strength calculated by EN 1993-1-4+A1 [13] and ANSI/AISC 370-21 [14].

*5.2. Evaluation of design approach in EN 1993-1-4+A1 [13]*

Fig. 18 illustrates a comparison between the design strength generated from EN 1993-1-4+A1 [13] and the results of both testing and parametric analysis, indicating that half of FE and test data are positioned below the design curves of EN 1993-1-4+A1 [13]. Moreover, the mean value of $V_{\mathrm{u,\,Test\,\&\,FE}}/V_{\mathrm{EN}}$ is 1.10, with a COV of 0.48. The design strength computed using EN 1993-1-4+A1 [13] is conservative by 10% on average, when compared with FE and test data, with a higher degree of scatter. Such a difference is due to the fact that the design rules given in EN 1993-1-4+A1 [13] do not consider the effect of perforations in the web, when computing the shear buckling capacity of stainless steel girders.

*5.3. Evaluation of design approach in ANSI/AISC 370-21 [14]*

Fig. 19 compares the design strength generated from ANSI/AISC 370-21 [14] with the test and parametric analysis results, indicating that half of FE and test data are positioned below the design curves of ANSI/AISC 370-21 [14]. The mean value of $V_{\mathrm{u,\,Test\,\&\,FE}}/V_{\mathrm{ANSI/AISC}}$ is 1.09, as depicted in Table 4. This indicates that the shear buckling capacity computed by ANSI/AISC 370-21 [14] is conservative by 9% on average, when compared with the FE and test data. The reason for the conservative prediction can be attributed to the fact that the design approaches presented in ANSI/AISC 370-21 [14] do not consider the impact of the end post conditions, which differs from those provided in EN 1993-1-4+A1 [13]. Moreover, it should be noted that the value of COV is up to 0.44, indicating that those FE and test data are scattered. The reason behind this is that the hole ratio ($d_w/h_w$) used in this parametric analysis is changed from 0.1 to 0.8, but the design rules given in ANSI/AISC 370-21 [14] are only designed for those specimens featuring unperforated webs.

Upon comparison, it was demonstrated that the EN 1993-1-4+A1 [13] and ANSI/AISC 370-21 [14] cannot provide accurate and safe predictions for determining the shear buckling capacity of such members. This indicated that new design rules for such perforated QN1803 members should be developed.

# 6. Conclusions and future work

This study presents six new laboratory tests, which were performed investigating the reduced shear buckling capacity of QN1803 stainless steel plate girders with perforated webs. The shear buckling capacity and failure mechanisms are obtained for all test specimens. The following conclusions may be generated from this investigation:

(1) A total of six new laboratory tests were performed, indicating that the shear buckling failures occurred at the web for all test specimens. Moreover, the tension bands developed in the web and the plastic hinge formed at the flanges. All of test specimens experienced a significant level of ductility prior to shear failure.

(2) The shear buckling capacity experienced a significant reduction due to the presence of web perforations, which was directly related to the hole ratio. For those members with a hole ratio of 0.6, the shear buckling capacity was reduced by 56% on average, compared to that of those members with unperforated webs.

(3) The distribution of the initial geometric imperfection was determined from three-dimensional (3D) scanning technique prior to the shear testing. The results revealed that the magnitude of these imperfections was lower than $h_w/200$ in most cases.

(4) Finite element models including both material nonlinearity and initial geometric imperfections were developed and validated using corresponding experimental results. A comparison between the test and numerical results was conducted and the results indicated that the mean value of $V_{u,Test}/V_{u,FEA}$ ratio is 0.98, with a coefficient of variation of 0.01. This indicated that the simulation results were in a good agreement with the test results.

(5) The generated test and FEA results were subsequently employed to assess the existing design approaches as specified in EN 1993-1-4+A1 (2015) and ANSI/AISC 370-21 (2021). Upon comparison, it was demonstrated that the design strength determined from EN 1993-1-4+A1 (2015) and ANSI/AISC 370-21 (2021) was over-conservative, when compared with the FE and test data, with a higher degree of scatter.

(6) The future work of this study is extending this work by performing a range of parametric analysis. Also, new design rules for closely predicting the shear buckling capacity of such perforated QN1803 members should be developed based on the results of parametric analysis.

## Acknowledgements

The authors would like to express their gratitude for the support offered by the National Natural Science Foundation of China (52208176), Shuimu Tsinghua Scholar Program (2021SM006), China Postdoctoral Science Foundation (2022M711860), China Postdoctoral International Exchange Program (YJ20220131), and Research Funding on Sustainable Development of Real Estate, Hang Lung Center for Real Estate, Tsinghua University (100002058). Special appreciations are extended to technical staffs from Beijing University of Civil Engineering and Architecture for their invaluable assistance in conducting experimental testing. Also, the assistance given by Dr. Dongdong Xu and Prof. Guowei Zhang is greatly appreciated.

## References


[1] Foshan Goldeco Stainless Steel Co. Ltd. Guangdong, China, 2022. https://www.goldecosteel.com/304d-stainless-steel.html.

[2] E. Real, E. Mirambell, I. Estrada, Shear response of stainless steel plate girders, Eng. Struct., 2007, 29 (7): 1626-1640.

[3] I. Estrada, E. Real, E. Mirambell, General behaviour and effect of rigid and non-rigid end post in stainless steel plate girders loaded in shear. Part I: experimental study, J. Constr. Steel Res., 2007, 63 (7): 970-984.

[4] I. Estrada, E. Real, E. Mirambell, General behaviour and effect of rigid and non-rigid end post in stainless steel plate girders loaded in shear. Part II: extended numerical study and design proposal, J. Constr. Steel Res., 2007, 63 (7): 985-996.

[5] N. Saliba, L. Gardner, Experimental study of shear response of lean duplex stainless steel plate girders, Eng. Struct., 2013, 46: 375-391.

[6] N. Saliba, E. Real, L. Gardner, Shear design recommendations for stainless steel plate girders, Eng. Struct., 2014, 59: 220-228.

[7] X.W. Chen, H.X. Yuan, X.X. Du, Y. Zhao, J. Ye, L. Yang, Shear buckling behaviour of welded stainless steel plate girders with transverse stiffeners, Thin-Walled Struct., 2018, 122: 529-544.

[8] B.S. Chen, Y.Q. Wang, D.D. Xu, H.X. Yuan, L.B. Yan, Shear performance and design rules for welded stainless steel I-shaped members with web openings, Thin-Walled Struct., 2023, 188:110803.

[9] B.S. Chen, Y.Q. Wang, Z.X. Wang, X.L. Liu, J.B.P. Lim, An experimental study on shear resistance of austenitic and duplex stainless steel plate girders with perforated webs, Eng. Struct., 2023, 295:116823.

[10] X.Y. Xue, X. Zhou, Y. Shi, Y. Xiang, Ultimate shear resistance of S600E high-strength stainless steel plate girders, J. Constr. Steel Res., 2021, 179: 106535.

[11] B.S. Chen, Y.Q. Wang, D.D. Xu, H.X. Yuan, L.B. Yan, Finite element analysis and proposed design rules for 304D high-strength stainless steel I-shaped members in shear, J. Constr. Steel Res., 2023, 204: 107861

[12] B.S. Chen, Y.Q. Wang, Z. Xing, J.B.P. Lim, L.T. Hai, Material properties and shear behaviour of QN1803 high-strength stainless steel plate girders, Eng. Struct.,2023, under revision.

[13] EN 1993-1-4+A1, Eurocode 3: Design of Steel Structures-Part 1.4: General Rules–supplementary Rules for Stainless Steel, CEN, 2015.

[14] ANSI/AISC 370-21, Specification for Structural Stainless Steel Buildings, American Institute of Steel Construction (AISC), Chicago, 2021.

[15] EN 1993-1-5, Eurocode 3: Design of Steel Structures-Part 1.5: Plated Structural Elements, CEN, 2006.

[16] ISO 6892-1: 2009. Metallic Materials -Tensile Testing-Part 1: Method of Test at Room Temperature. International Organization for Standardization, Geneva, Switzerland, 2009.

[17] D.D. Xu., Y.Q. Wang, X.L. Liu. B.S. Chen, Y.D. Bu., A novel method and modelling technique for determining the initial geometric imperfection of steel members using 3D scanning, Struct., 2023, 49: 855-874.

[18] ABAQUS Analysis User's Manual-Version 6.14-2, ABAQUS Inc., USA, 2018.

[19] R. Feng, J. Liu, Z. Chen, K. Roy, B.S. Chen, J.B.P. Lim, Numerical investigation and design rules for flexural capacities of H-section high-strength steel beams with and without web openings, Eng. Struct., 2020, 225: 111278.

[20] B.S. Chen, K. Roy, Z. Fang, A. Uzzaman, C. H. Pham, G. Raftery, J.B.P. Lim. Shear capacity of cold-formed steel channels with edge-stiffened web holes, un-stiffened web holes, and plain webs, J. Struct. Eng.-ASCE, 2022, 148(2): 04021268.

[21] R. Feng, Z.P. Huang, Z.M. Chen, K. Roy, B.S. Chen, J.B.P. Lim, Finite-element analysis and design of stainless-steel CHS-to-SHS hybrid tubular joints under axial compression, Thin-Walled Struct., 2020, 151: 106728.

[22] L. Gardner, M. Ashraf, Structural design for non-linear metallic material, Eng. Struct. 2006,28 (6):926-934.

## Table 1 Measured geometric dimensions and key results

| Specimen ID | Material grade | $L$/mm | $h_w$/mm | $a$/mm | $t_w$/mm | $t_f$/mm | $d_{wh}/mm$ | $w_0/mm$ | $d_w/h_w$ | $a/h_w$ | End case | $V_{u,Test}$/kN | $V_{u,FEA}$/kN | $V_{u,Test}/V_{u,FEA}$ |
|---|---|---|---|---|---|---|---|---|---|---|---|---|---|---|
| **Unperforated web [12]** | | | | | | | | | | | | | | |
| V304D-H500-ad1.0-A0 | QN1803 | 1200.7 | 499.3 | 498.5 | 3.67 | 11.76 | 0 | 3.10 | 0 | 1.0 | Non-rigid | 344.26 | 349.87 | 0.98 |
| V304D-H700-ad1.0-A0 | QN1803 | 1600.1 | 697.2 | 699.3 | 3.68 | 11.81 | 0 | 5.30 | 0 | 1.0 | Non-rigid | 367.15 | 371.78 | 0.99 |
| **Perforated web** | | | | | | | | | | | | | | |
| V304D-H500-ad1.0-A0.2 | QN1803 | 1199.8 | 498.5 | 499.3 | 3.61 | 11.78 | 101.5 | 1.5 | 0.2 | 1.0 | Non-rigid | 296.02 | 300.67 | 0.98 |
| V304D-H500-ad1.0-A0.4 | QN1803 | 1200.8 | 499.1 | 499.0 | 3.52 | 11.82 | 200.3 | 1.5 | 0.4 | 1.0 | Non-rigid | 232.65 | 235.63 | 0.99 |
| V304D-H500-ad1.0-A0.6 | QN1803 | 1201.2 | 498.5 | 499.2 | 3.68 | 11.80 | 300.5 | 1.4 | 0.6 | 1.0 | Non-rigid | 151.15 | 152.63 | 0.99 |
| V304D-H500-ad1.0-A0.6-R | QN1803 | 1200.3 | 499.1 | 498.6 | 3.67 | 11.90 | 301.2 | 2.3 | 0.6 | 1.0 | Rigid | 154.39 | 158.51 | 0.97 |
| V304D-H500-ad1.5-A0.6 | QN1803 | 1702.3 | 498.6 | 748.9 | 3.64 | 11.81 | 300.3 | 3.8 | 0.6 | 1.5 | Non-rigid | 123.42 | 124.76 | 0.99 |
| V304D-H700-ad1.0-A0.6 | QN1803 | 1600.1 | 698.8 | 699.5 | 3.67 | 11.80 | 420.5 | 3.1 | 0.6 | 1.0 | Non-rigid | 167.85 | 168.85 | 0.99 |
| Mean | | | | | | | | | | | | | | 0.98 |
| COV | | | | | | | | | | | | | | 0.01 |

## Table 2 Material properties obtained from tensile coupon tests [12]

| Grades | Coupon ID | Thickness $t_w$/mm | Young's modulus $E_0$/GPa | Yield stress $\sigma_{0.2}$/MPa | Ultimate stress $\sigma_u$/MPa |
|---|---|---|---|---|---|
| Austenitic QN1803 | 304D-T4-1 | 3.70 | 196.0 | 481.1 | 767.0 |
| | 304D-T4-2 | 3.67 | 198.5 | 480.4 | 777.4 |
| | 304D-T4-3 | 3.70 | 195.8 | 470.6 | 776.6 |
| | 304D-T12-1 | 11.75 | 198.0 | 411.0 | 736.1 |
| | 304D-T12-2 | 11.79 | 199.5 | 418.8 | 734.5 |
| | 304D-T12-3 | 11.73 | 199.8 | 429.1 | 739.7 |

**Table 3 Range of key parameters used in the parametric analysis**

| Key parameters | Range | Quantity |
|---|---|---|
| Web aspect ratio ($a/h_w$) | 0.75, 1.0, 1.5 | 62 |
| Height-thickness ratio ($h_w/t_w$) | 100, 200, 300, 400 | 62 |
| Hole diameter-web height ratio ($d_{wh}/h_w$) | 0.1, 0 0.5, 0.6, 0.7,0.8 | 62 |
| End post conditions | Non-rigid, rigid | 32 |

**Table 4 Comparison of test and FEA results with the existing design methods**

| Specimen ID | Key parameters | | | | Test & FE (kN) | Existing design methods (kN) | | Test & FE /existing design methods | |
|---|---|---|---|---|---|---|---|---|---|
| | End post | $h_w/t_w$ | $d_{wh}/h_w$ | $a/h_w$ | $V_{u,Test\&FE}$ | $V_{EN}$ | $V_{ANSI/AISC}$ | $V_{u,Test\&FE}/V_{EN}$ | $V_{u,Test\&FE}/V_{ANSI/AISC}$ |
| **Experiments** | | | | | | | | | |
| H500-ad1.0-A0.2 | N | 138.09 | 0.2 | 1.0 | 296.02 | 260.95 | 271.10 | 1.13 | 1.09 |
| H500-ad1.0-A0.4 | N | 141.79 | 0.4 | 1.0 | 232.65 | 249.66 | 259.36 | 0.93 | 0.90 |
| H500-ad1.0-A0.6 | N | 135.46 | 0.6 | 1.0 | 151.15 | 269.92 | 280.42 | 0.56 | 0.54 |
| H500-ad1.5-A0.6 | N | 136.98 | 0.6 | 1.5 | 123.42 | 238.43 | 247.66 | 0.52 | 0.50 |
| H700-ad1.0-A0.6 | N | 190.41 | 0.6 | 1.0 | 167.85 | 288.63 | 299.75 | 0.58 | 0.56 |
| H500-ad1.0-A0.6-R | R | 135.99 | 0.6 | 1.0 | 154.39 | 302.24 | 279.16 | 0.51 | 0.55 |
| **Parametric study** | | | | | | | | | |
| H600-ad1.0-A0.5 | N | 100 | 0.5 | 1.0 | 147.96 | 73.42 | 76.31 | 2.02 | 1.94 |
| H1000-ad1.0-A0.5 | N | 200 | 0.5 | 1.0 | 117.29 | 86.49 | 89.81 | 1.36 | 1.31 |
| H1400-ad1.0-A0.5 | N | 300 | 0.5 | 1.0 | 115.77 | 91.94 | 95.44 | 1.26 | 1.21 |
| H1800-ad1.0-A0.5 | N | 400 | 0.5 | 1.0 | 123.91 | 94.93 | 98.53 | 1.31 | 1.26 |
| H800-ad1.5-A0.5 | N | 100 | 0.5 | 1.5 | 111.96 | 66.65 | 69.26 | 1.68 | 1.62 |
| H1400-ad1.5-A0.5 | N | 200 | 0.5 | 1.5 | 92.09 | 77.25 | 80.21 | 1.19 | 1.15 |
| H2000-ad1.5-A0.5 | N | 300 | 0.5 | 1.5 | 92.69 | 81.57 | 84.67 | 1.14 | 1.09 |
| H800-ad0.75-A0.5 | N | 200 | 0.5 | 0.75 | 120.16 | 100.35 | 104.22 | 1.20 | 1.15 |
| H1000-ad1.0-A0.1 | N | 200 | 0.1 | 1.0 | 183.83 | 86.49 | 89.81 | 2.13 | 2.05 |
| H1400-ad1.0-A0.1 | N | 300 | 0.1 | 1.0 | 145.64 | 91.94 | 95.44 | 1.58 | 1.53 |
| H1800-ad1.0-A0.1 | N | 400 | 0.1 | 1.0 | 172.75 | 94.93 | 98.53 | 1.82 | 1.75 |
| H800-ad1.5-A0.1 | N | 100 | 0.1 | 1.5 | 147.12 | 66.65 | 69.26 | 2.21 | 2.12 |
| H1400-ad1.5-A0.1 | N | 200 | 0.1 | 1.5 | 141.78 | 77.25 | 80.21 | 1.84 | 1.77 |
| H2000-ad1.5-A0.1 | N | 300 | 0.1 | 1.5 | 147.31 | 81.57 | 84.67 | 1.81 | 1.74 |
| H800-ad0.75-A0.1 | N | 200 | 0.1 | 0.75 | 210.35 | 100.35 | 104.22 | 2.10 | 2.02 |
| H1100-ad0.75-A0.1 | N | 300 | 0.1 | 0.75 | 211.78 | 107.76 | 111.88 | 1.97 | 1.89 |
| H1400-ad0.75-A0.1 | N | 400 | 0.1 | 0.75 | 217.20 | 111.90 | 116.15 | 1.94 | 1.87 |
| H600-ad1.0-A0.7 | N | 100 | 0.7 | 1.0 | 120.94 | 73.42 | 76.31 | 1.65 | 1.58 |
| H1000-ad1.0-A0.7 | N | 200 | 0.7 | 1.0 | 71.33 | 86.49 | 89.81 | 0.82 | 0.79 |
| H1400-ad1.0-A0.7 | N | 300 | 0.7 | 1.0 | 71.11 | 91.94 | 95.44 | 0.77 | 0.75 |
| H1800-ad1.0-A0.7 | N | 400 | 0.7 | 1.0 | 54.33 | 94.93 | 98.53 | 0.57 | 0.55 |
| H800-ad1.5-A0.7 | N | 100 | 0.7 | 1.5 | 94.45 | 66.65 | 69.26 | 1.42 | 1.36 |
| H1400-ad1.5-A0.7 | N | 200 | 0.7 | 1.5 | 64.33 | 77.25 | 80.21 | 0.83 | 0.80 |
| H2000-ad1.5-A0.7 | N | 300 | 0.7 | 1.5 | 50.14 | 81.57 | 84.67 | 0.61 | 0.59 |
| H500-ad0.75-A0.7 | N | 100 | 0.7 | 0.75 | 152.59 | 83.17 | 86.46 | 1.83 | 1.76 |
| H800-ad0.75-A0.7 | N | 200 | 0.7 | 0.75 | 71.26 | 100.35 | 104.22 | 0.71 | 0.68 |
| H1100-ad0.75-A0.7 | N | 300 | 0.7 | 0.75 | 67.82 | 107.76 | 111.88 | 0.63 | 0.61 |
| H1400-ad0.75-A0.7 | N | 400 | 0.7 | 0.75 | 74.06 | 111.90 | 116.15 | 0.66 | 0.64 |
| H600-ad1.0-A0.8 | N | 100 | 0.8 | 1.0 | 117.02 | 73.42 | 76.31 | 1.59 | 1.53 |
| H1000-ad1.0-A0.8 | N | 200 | 0.8 | 1.0 | 42.63 | 86.49 | 89.81 | 0.49 | 0.47 |
| H1400-ad1.0-A0.8 | N | 300 | 0.8 | 1.0 | 41.52 | 91.94 | 95.44 | 0.45 | 0.44 |
| H1800-ad1.0-A0.8 | N | 400 | 0.8 | 1.0 | 43.61 | 94.93 | 98.53 | 0.46 | 0.44 |
| H800-ad1.5-A0.8 | N | 100 | 0.8 | 1.5 | 53.53 | 66.65 | 69.26 | 0.80 | 0.77 |
| H1400-ad1.5-A0.8 | N | 200 | 0.8 | 1.5 | 41.48 | 77.25 | 80.21 | 0.54 | 0.52 |
| H2000-ad1.5-A0.8 | N | 300 | 0.8 | 1.5 | 35.59 | 81.57 | 84.67 | 0.44 | 0.42 |
| H600-ad1.0-A0.6 | N | 100 | 0.6 | 1.0 | 137.11 | 73.42 | 76.31 | 1.87 | 1.80 |
| H1000-ad1.0-A0.6 | N | 200 | 0.6 | 1.0 | 97.78 | 86.49 | 89.81 | 1.13 | 1.09 |
| H1400-ad1.0-A0.6 | N | 300 | 0.6 | 1.0 | 93.32 | 91.94 | 95.44 | 1.01 | 0.98 |
| H1800-ad1.0-A0.6 | N | 400 | 0.6 | 1.0 | 62.13 | 94.93 | 98.53 | 0.65 | 0.63 |
| H800-ad1.5-A0.6 | N | 100 | 0.6 | 1.5 | 102.16 | 66.65 | 69.26 | 1.53 | 1.48 |

| | | | | | | | | | |
|---|---|---|---|---|---|---|---|---|---|
| H1400-ad1.5-A0.6 | N | 200 | 0.6 | 1.5 | 74.02 | 77.25 | 80.21 | 0.96 | 0.92 |
| H2000-ad1.5-A0.6 | N | 300 | 0.6 | 1.5 | 73.36 | 81.57 | 84.67 | 0.90 | 0.87 |
| H800-ad0.75-A0.6 | N | 200 | 0.6 | 0.75 | 95.46 | 100.35 | 104.22 | 0.95 | 0.92 |
| H1100-ad0.75-A0.6 | N | 300 | 0.6 | 0.75 | 84.43 | 107.76 | 111.88 | 0.78 | 0.75 |
| H1400-ad0.75-A0.6 | N | 400 | 0.6 | 0.75 | 85.61 | 111.90 | 116.15 | 0.77 | 0.74 |
| H1000-ad1.0-A0.5 | R | 200 | 0.5 | 1.0 | 123.54 | 101.05 | 89.81 | 1.22 | 1.38 |
| H1400-ad1.0-A0.5 | R | 300 | 0.5 | 1.0 | 125.69 | 110.94 | 95.44 | 1.13 | 1.32 |
| H1800-ad1.0-A0.5 | R | 400 | 0.5 | 1.0 | 131.83 | 116.64 | 98.53 | 1.13 | 1.34 |
| H1400-ad1.5-A0.5 | R | 200 | 0.5 | 1.5 | 102.93 | 91.32 | 80.21 | 1.13 | 1.28 |
| H2000-ad1.5-A0.5 | R | 300 | 0.5 | 1.5 | 96.24 | 99.31 | 84.67 | 0.97 | 1.14 |
| H800-ad0.75-A0.5 | R | 200 | 0.5 | 0.75 | 140.17 | 115.24 | 104.22 | 1.25 | 1.38 |
| H1100-ad0.75-A0.5 | R | 300 | 0.5 | 0.75 | 101.61 | 128.27 | 111.88 | 0.79 | 0.91 |
| H600-ad1.0-A0.7 | R | 100 | 0.7 | 1.0 | 128.02 | 79.74 | 76.31 | 1.61 | 1.68 |
| H1000-ad1.0-A0.7 | R | 200 | 0.7 | 1.0 | 78.78 | 101.05 | 89.81 | 0.78 | 0.88 |
| H1400-ad1.0-A0.7 | R | 300 | 0.7 | 1.0 | 77.11 | 110.94 | 95.44 | 0.70 | 0.81 |
| H1800-ad1.0-A0.7 | R | 400 | 0.7 | 1.0 | 58.65 | 116.64 | 98.53 | 0.50 | 0.60 |
| H800-ad1.5-A0.7 | R | 100 | 0.7 | 1.5 | 98.45 | 73.55 | 69.26 | 1.34 | 1.42 |
| H1400-ad1.5-A0.7 | R | 200 | 0.7 | 1.5 | 68.70 | 91.32 | 80.21 | 0.75 | 0.86 |
| H2000-ad1.5-A0.7 | R | 300 | 0.7 | 1.5 | 54.44 | 99.31 | 84.67 | 0.55 | 0.64 |
| H800-ad0.75-A0.7 | R | 200 | 0.7 | 0.75 | 80.16 | 115.24 | 104.22 | 0.70 | 0.77 |
| H1100-ad0.75-A0.7 | R | 300 | 0.7 | 0.75 | 83.86 | 128.27 | 111.88 | 0.68 | 0.78 |
| H1400-ad0.75-A0.7 | R | 400 | 0.7 | 0.75 | 86.86 | 135.96 | 116.15 | 0.64 | 0.75 |
| Mean | | | | | | | | 1.10 | 1.09 |
| COV | | | | | | | | 0.48 | 0.44 |

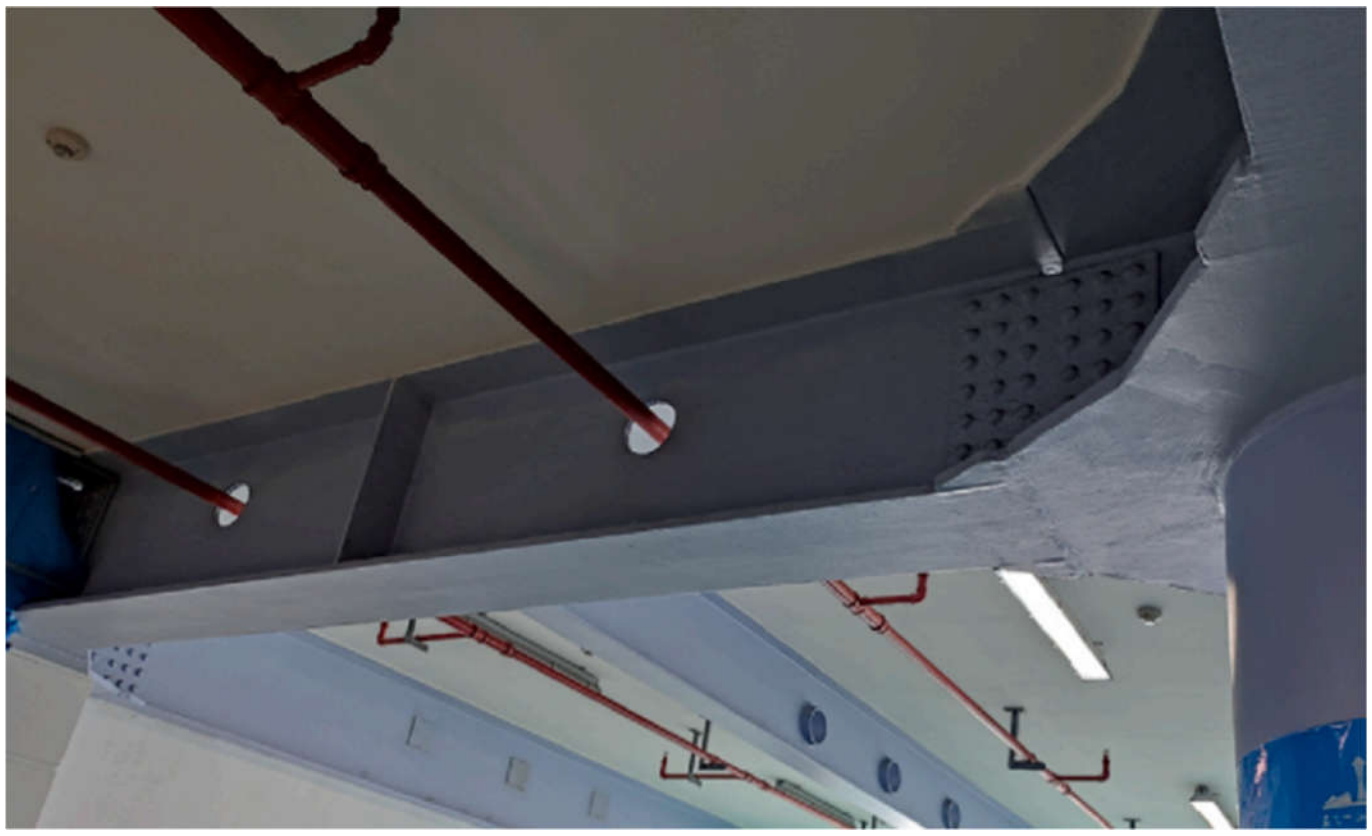

**Fig. 1. Engineering application of perforated plate girders**

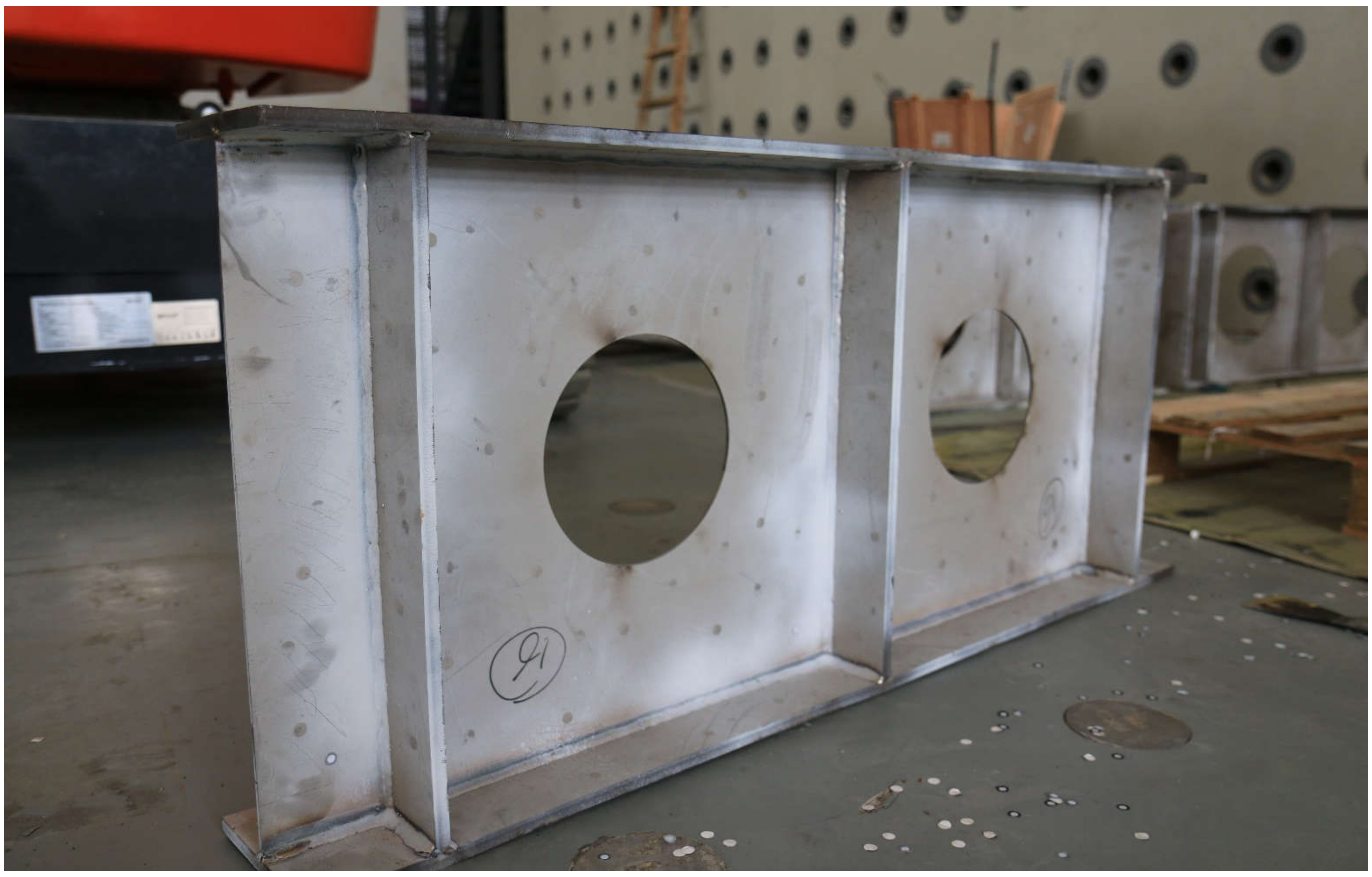

(a) Photograph of test specimen

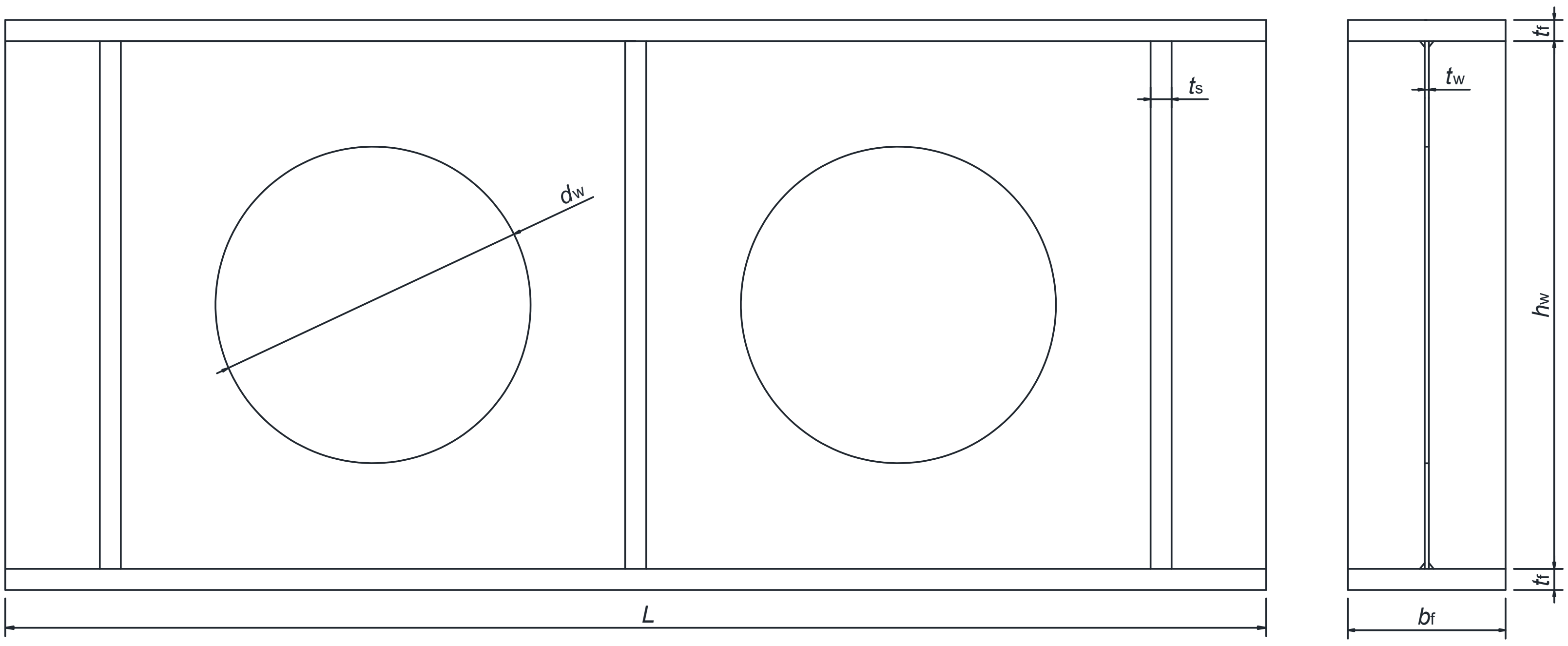


(b) Geometry of test specimen containing free-end posts

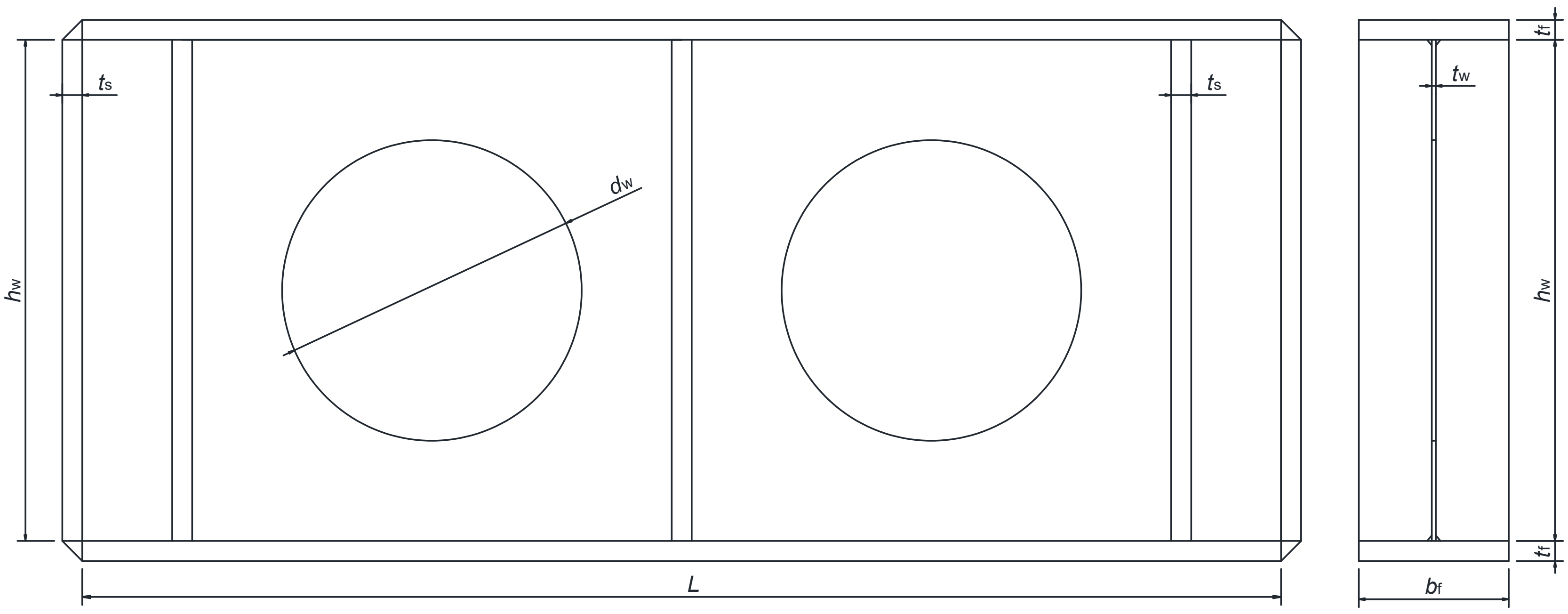


(c) Geometry of test specimen containing strengthened-end posts

**Fig. 2. QN1803 stainless steel plate girders with perforated webs**

(a) Photograph of test setup

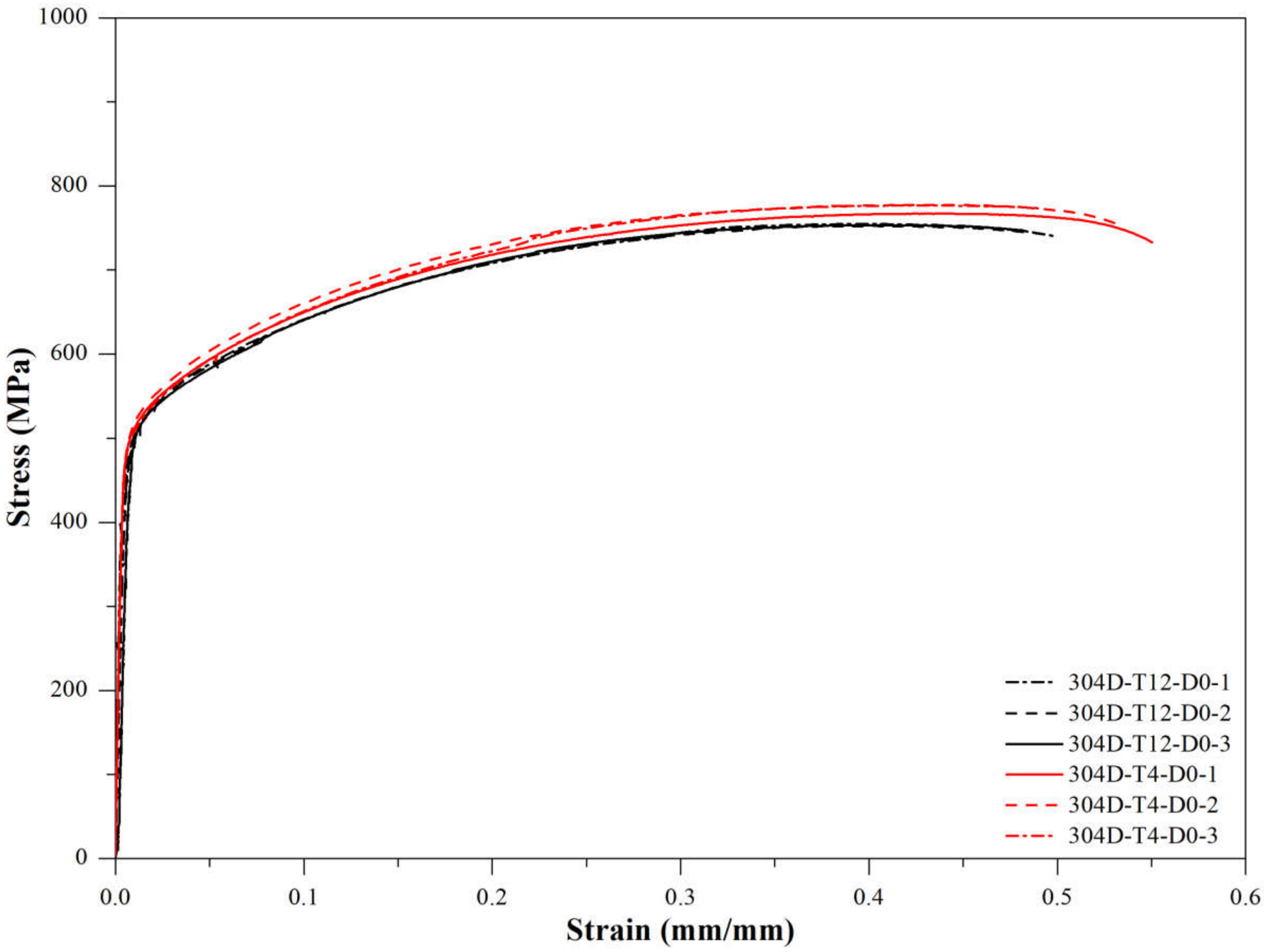


(b) Full-range stress-strain curves

**Fig. 3. Tensile coupon tests**

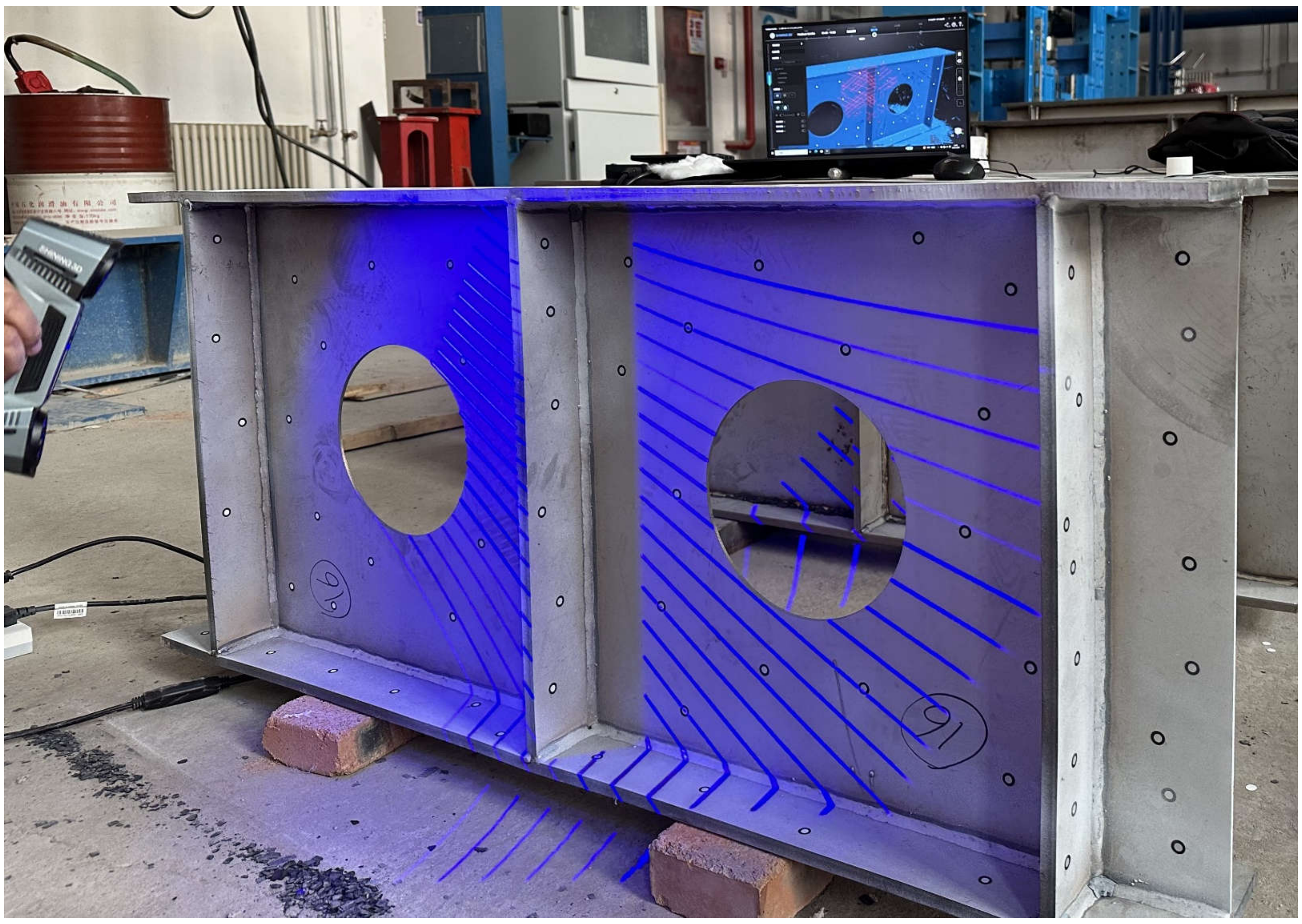

(a) Photograph

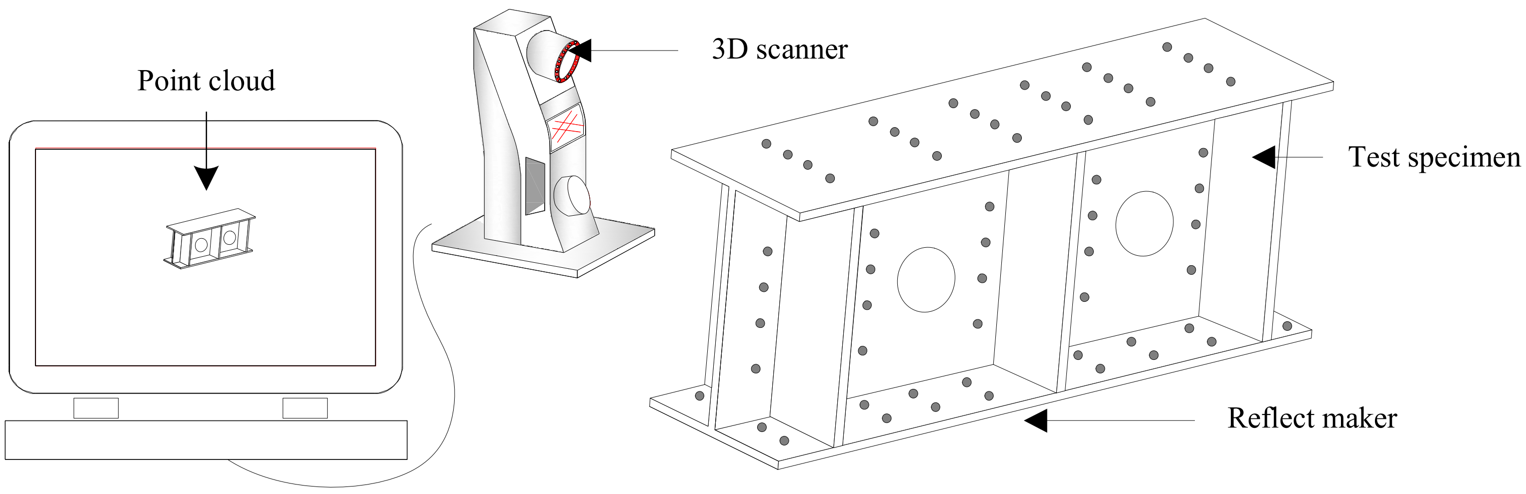


(b) Schematic diagram

**Fig. 4. 3D laser scanning device and the operating procedures**

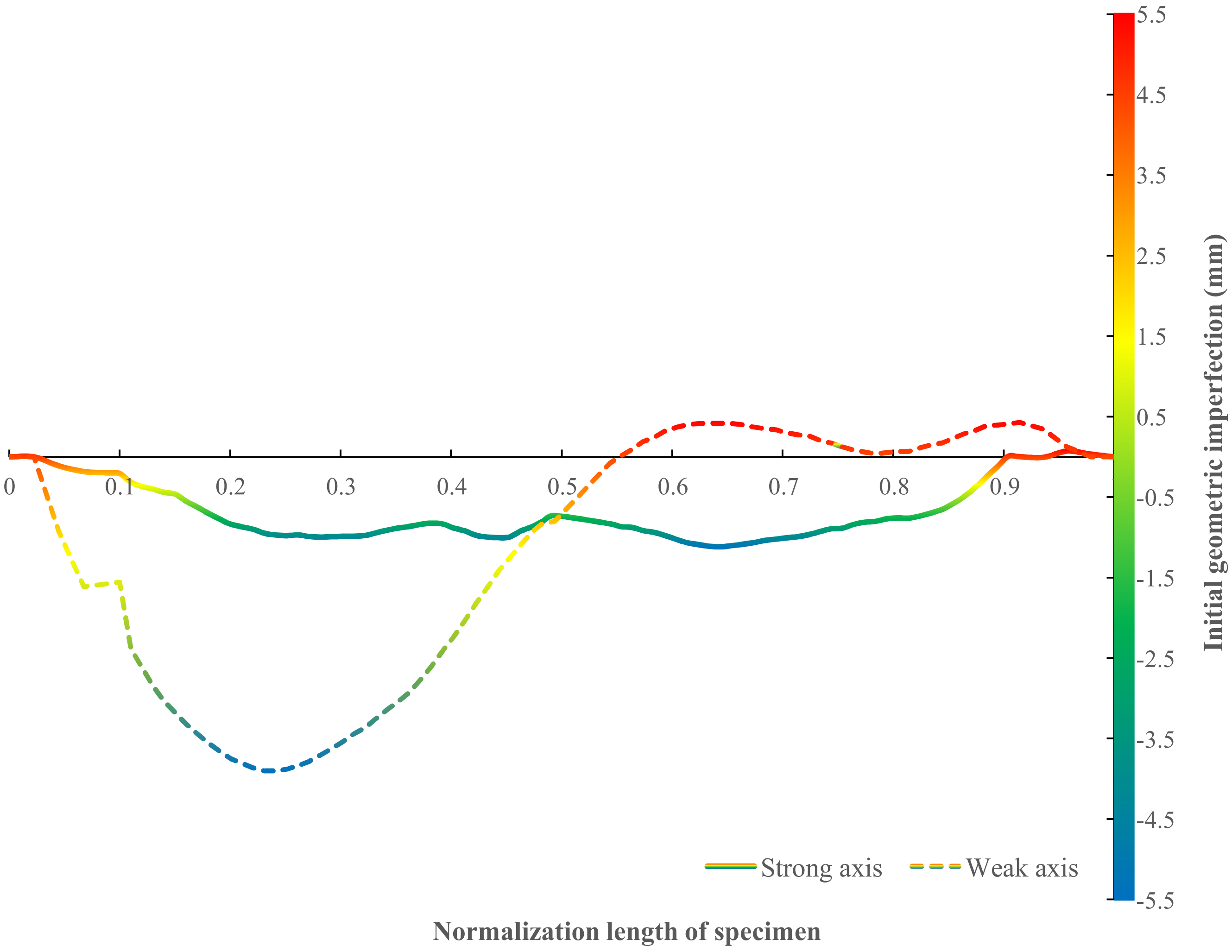


(a) V304D-H500-ad1.0-A0.4

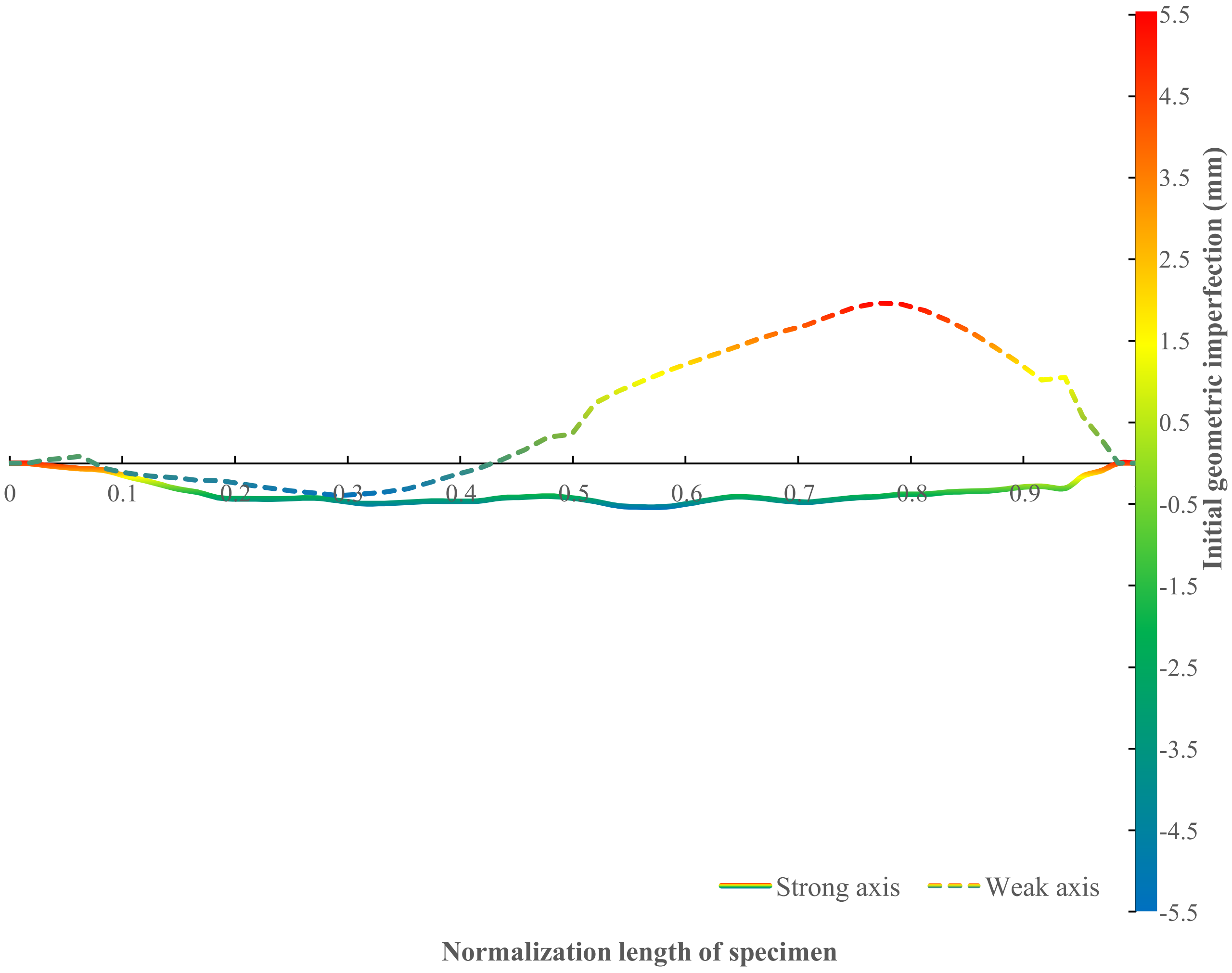


(b) V304D-H500-ad1.0-A0.6

**Fig. 5. Measured initial imperfection along the length direction**

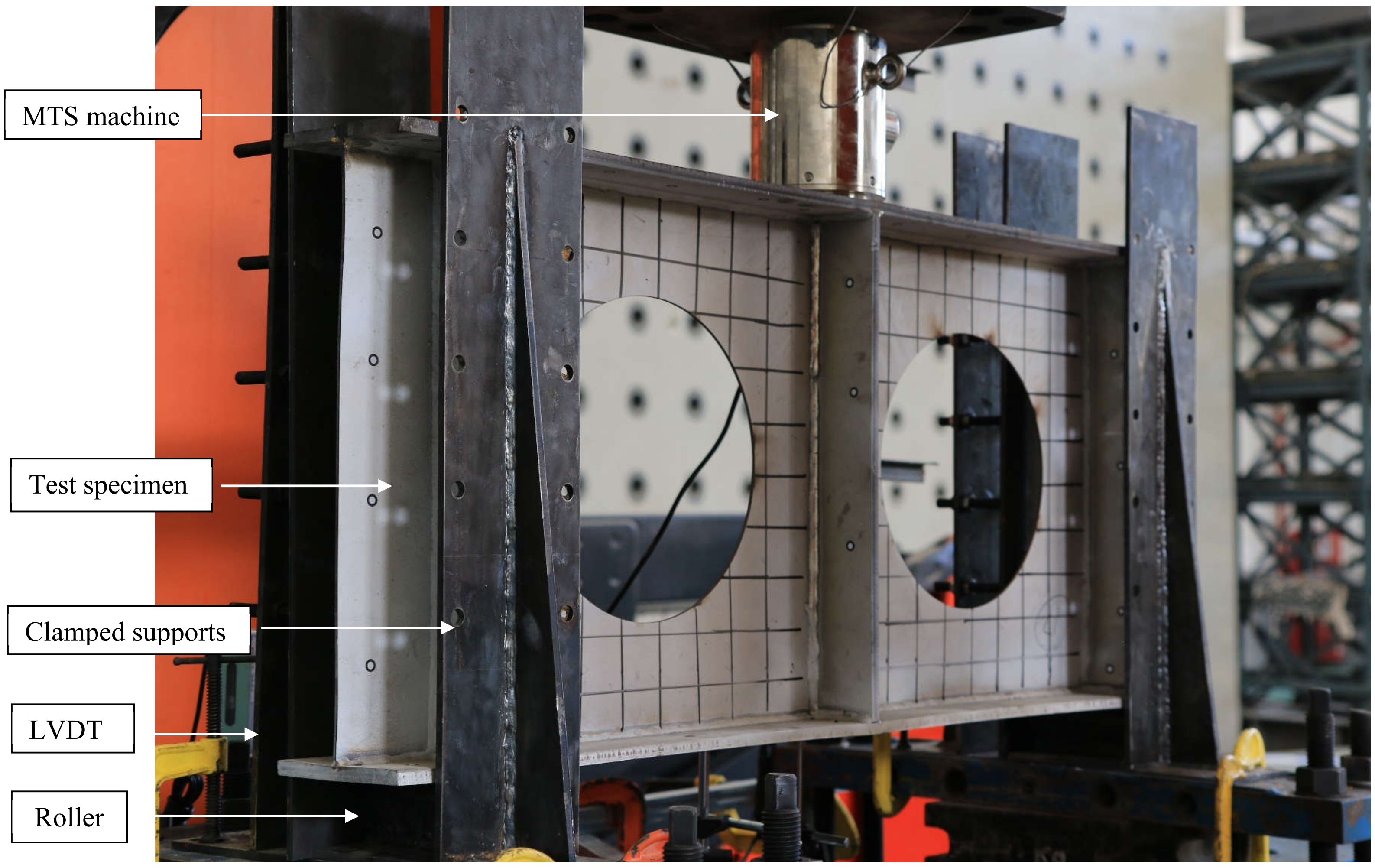


(a) Photograph of shear tests

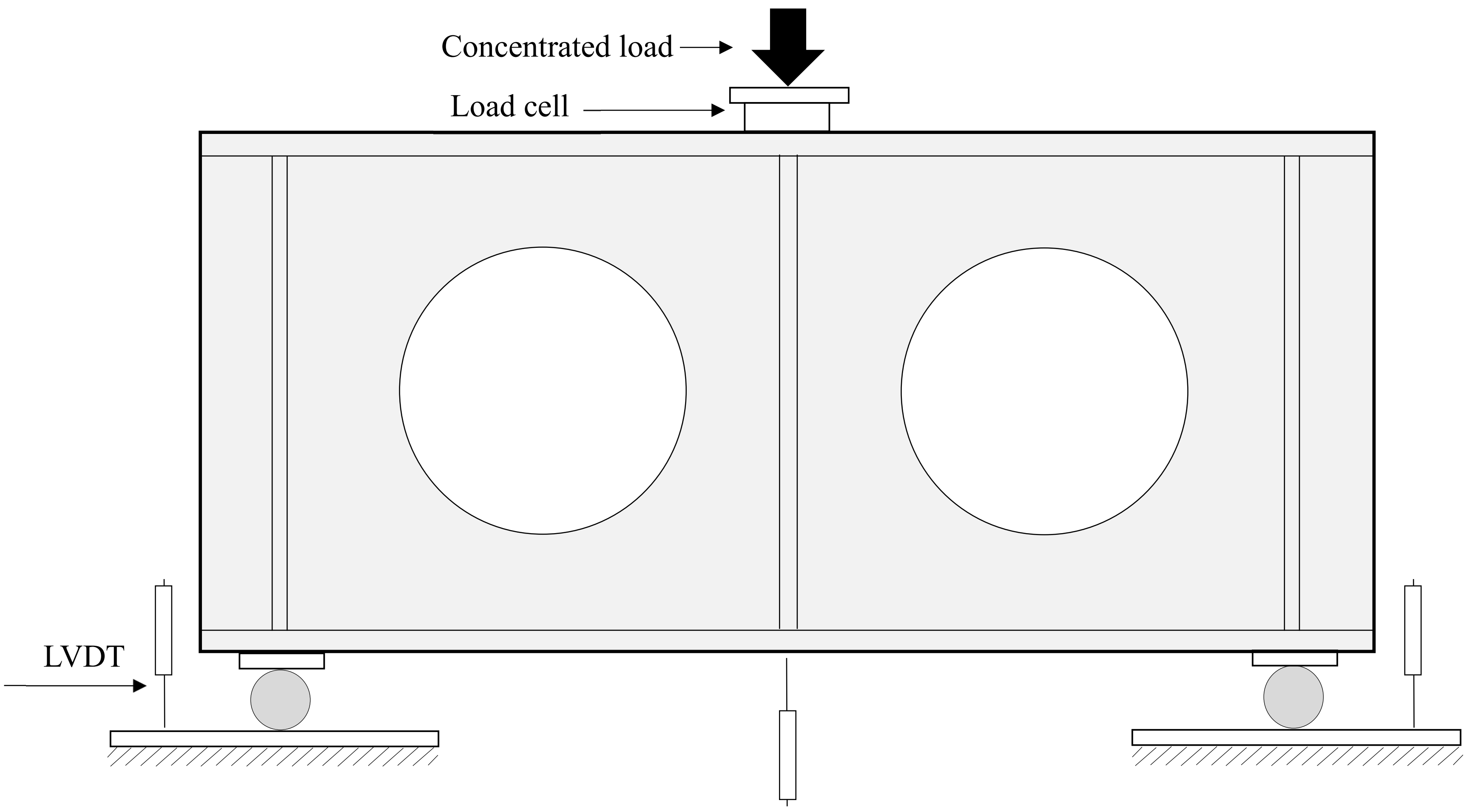


(b) Schematic diagram

**Fig. 6. Testing setup of shear tests**

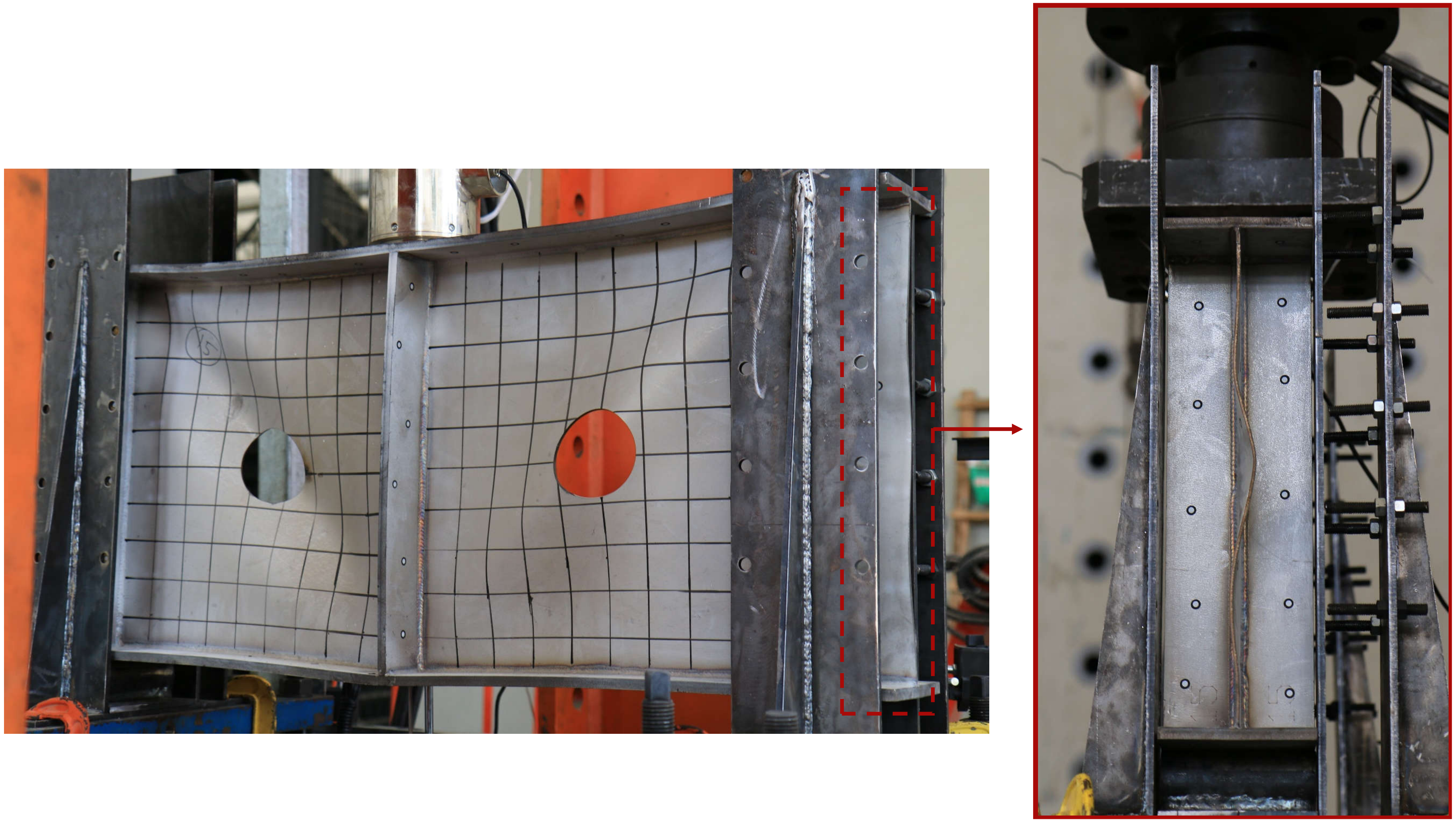

**Fig. 7. Deformed shapes of test specimen V304D-H500-ad1.0-A0.2**

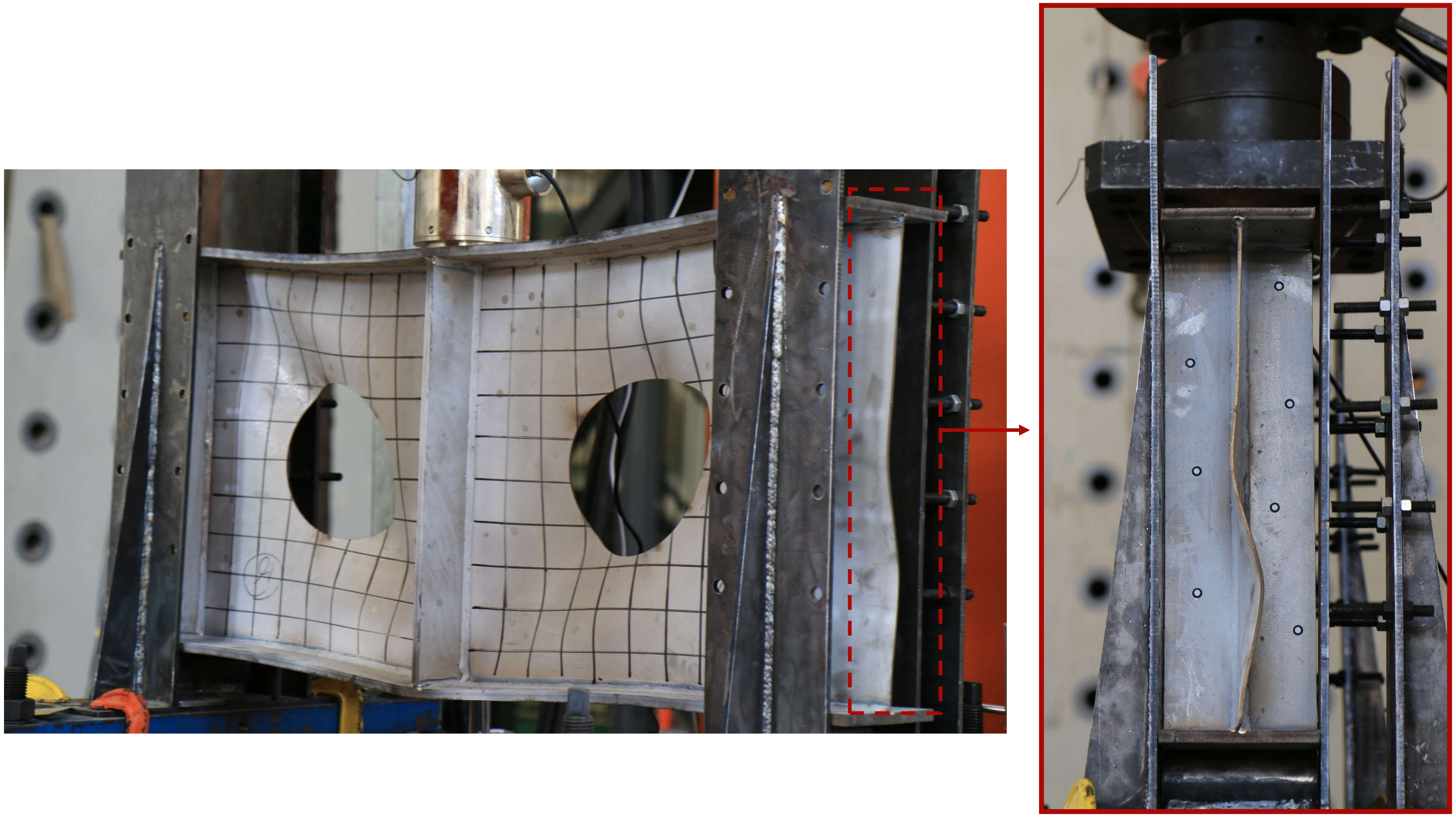

**Fig. 8. Deformed shapes of test specimen V304D-H500-ad1.0-A0.4**

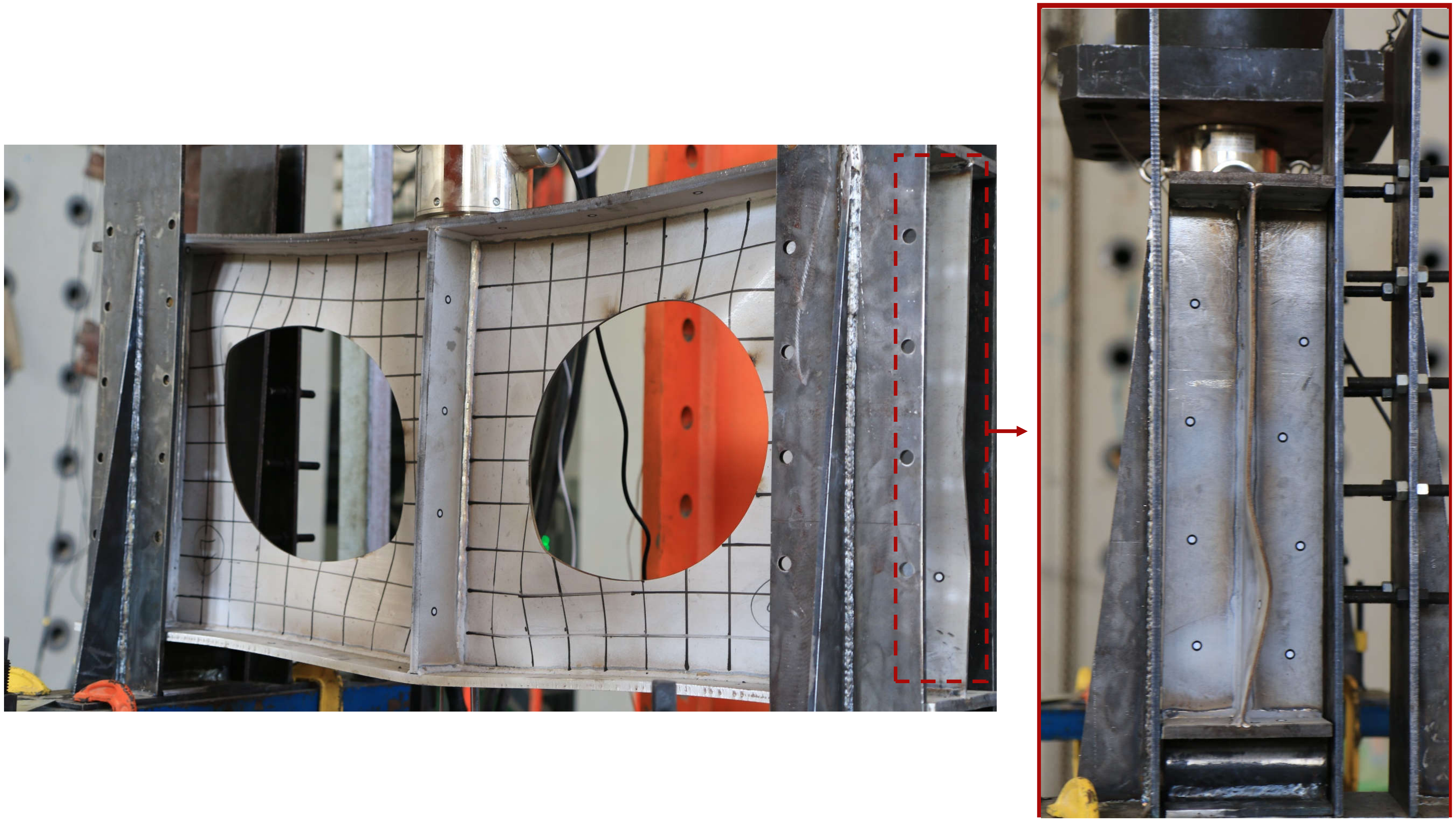

**Fig. 9. Deformed shapes of test specimen V304D-H500-ad1.0-A0.6**

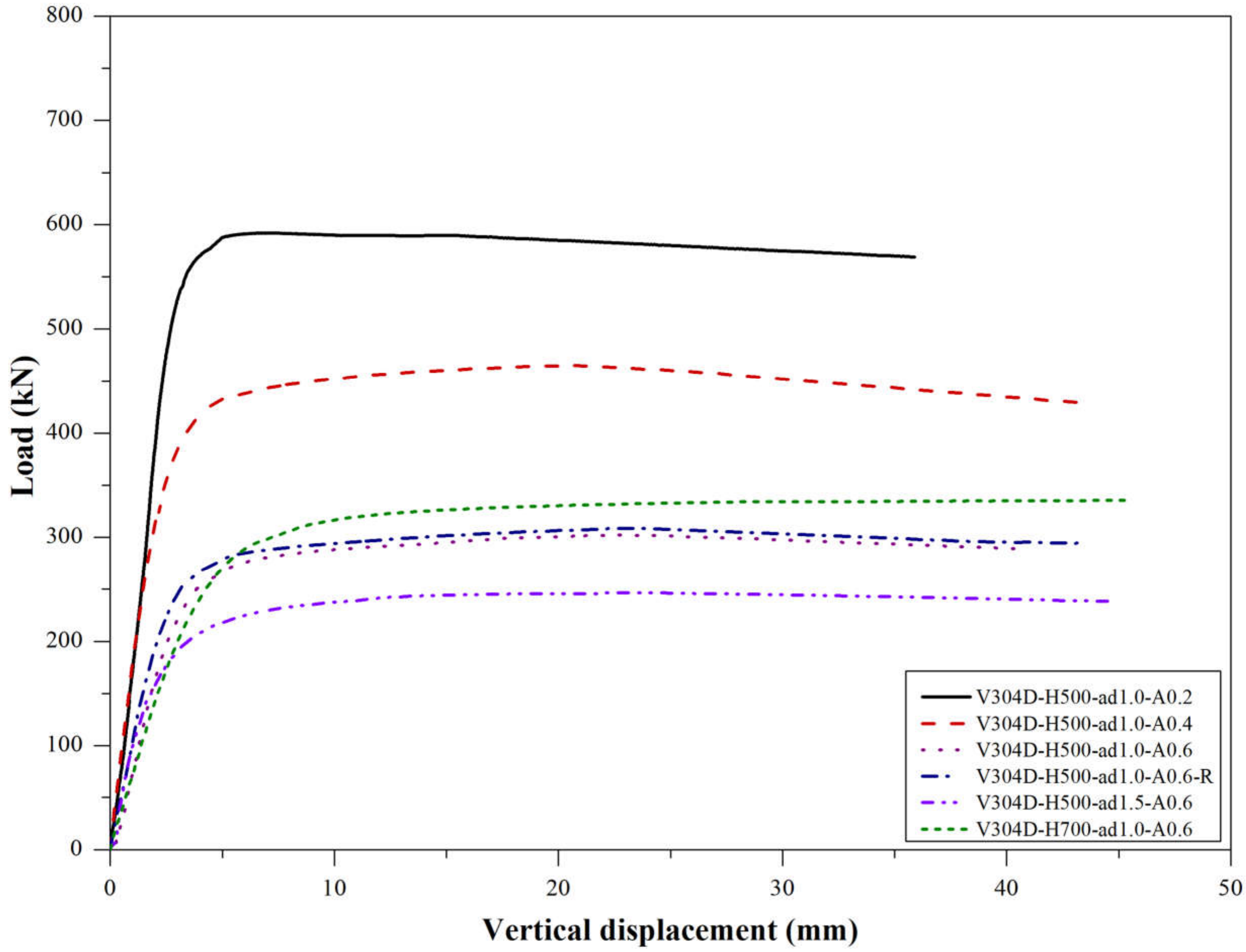


**Fig. 10. Ultimate strength versus vertical displacement of all test specimens**

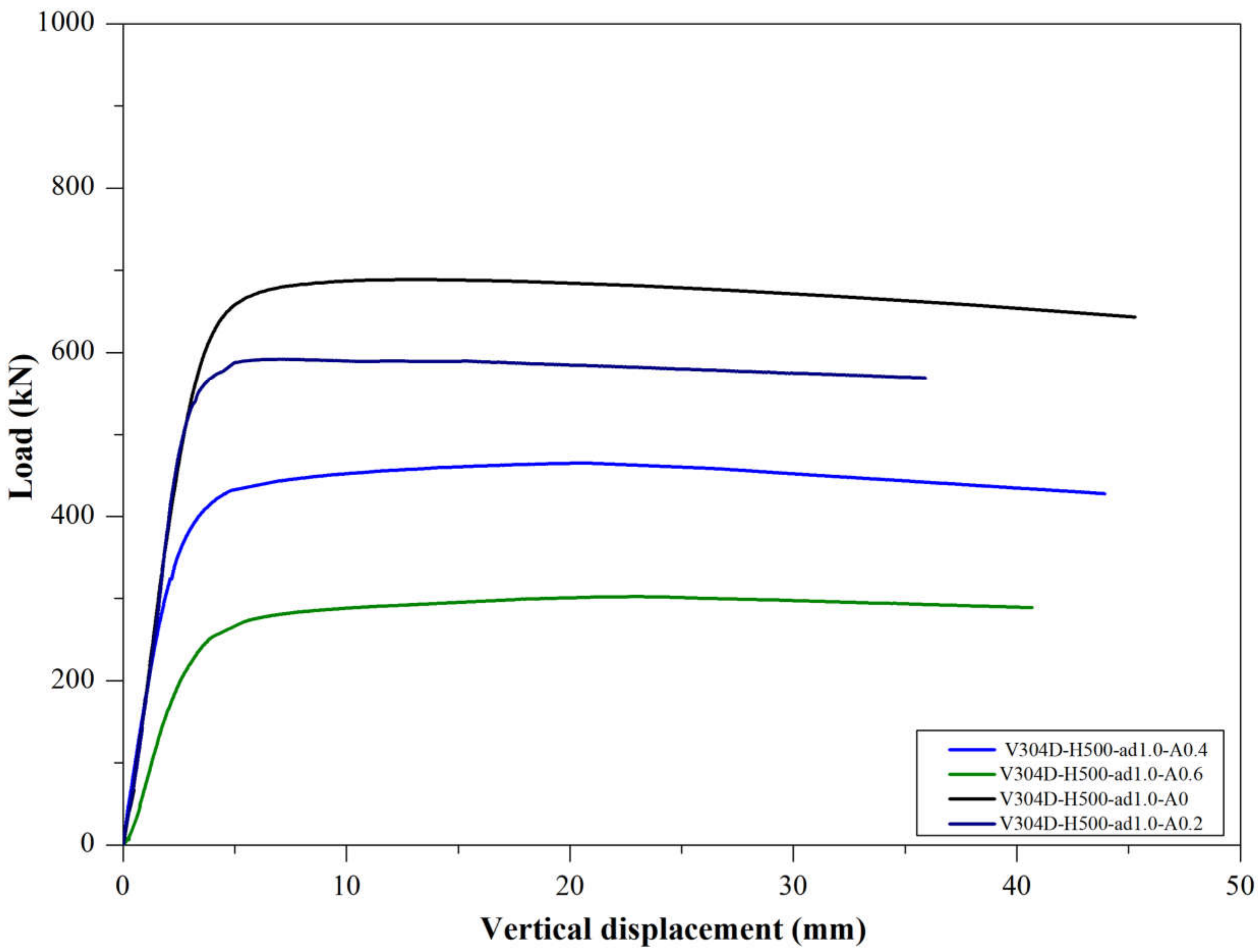


**Fig. 11. Effect of web perforation on ultimate strength**

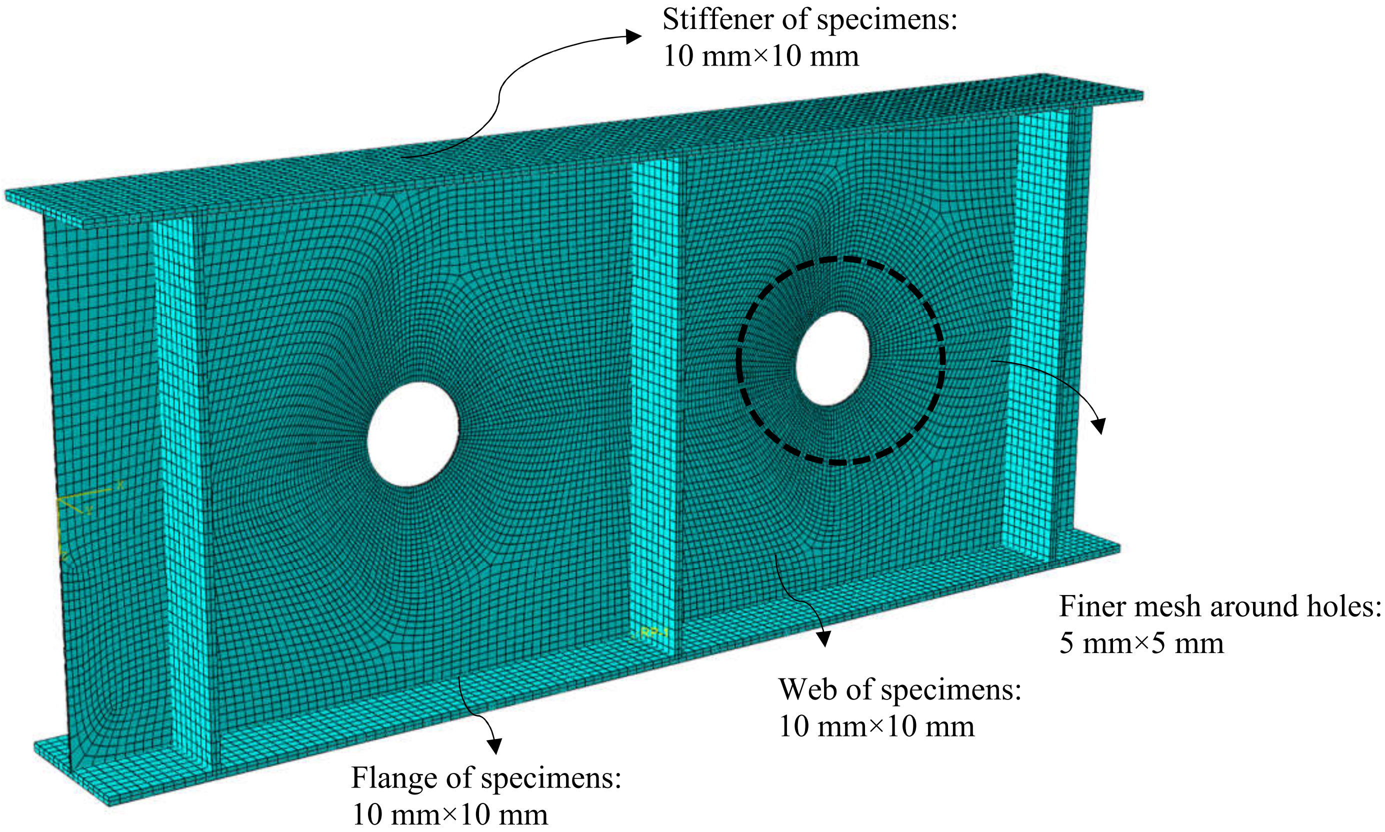


(a) Mesh size

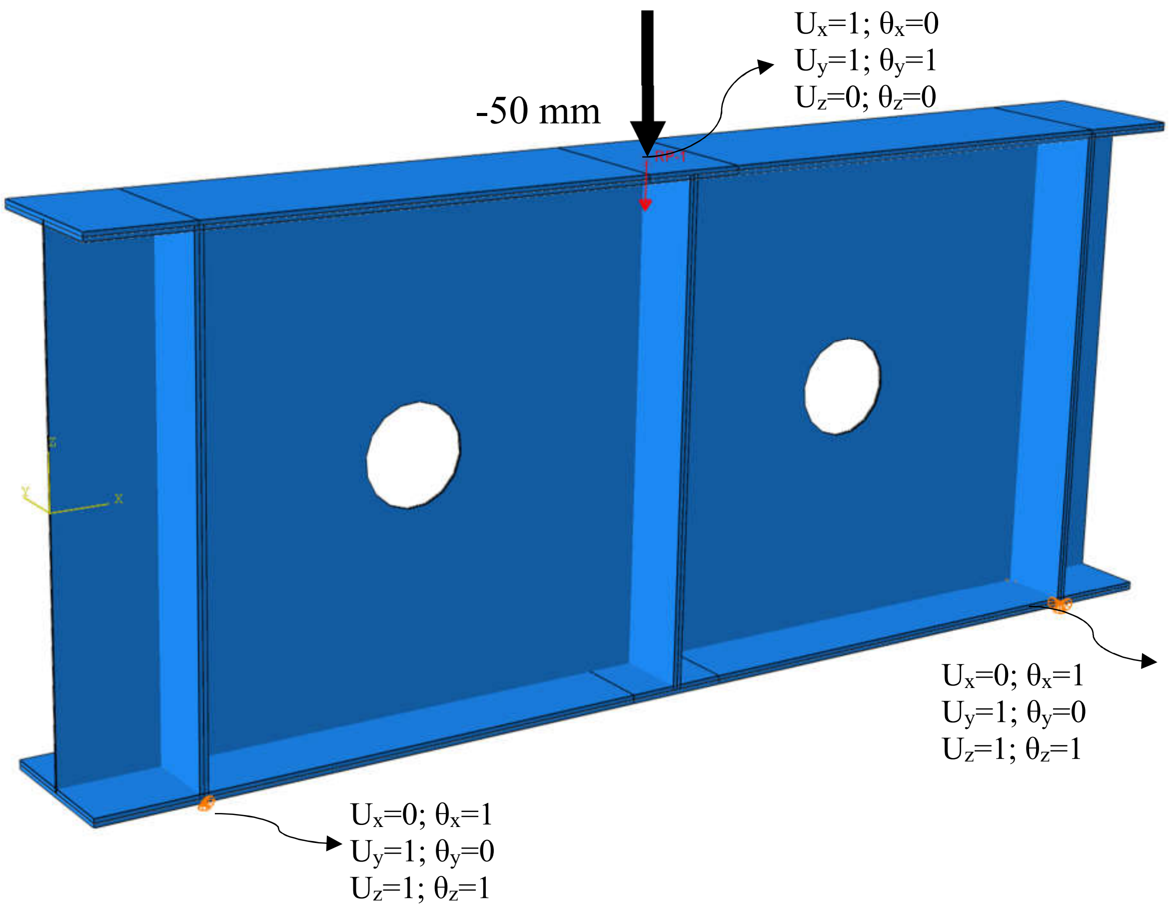


(b) Loading and boundary conditions

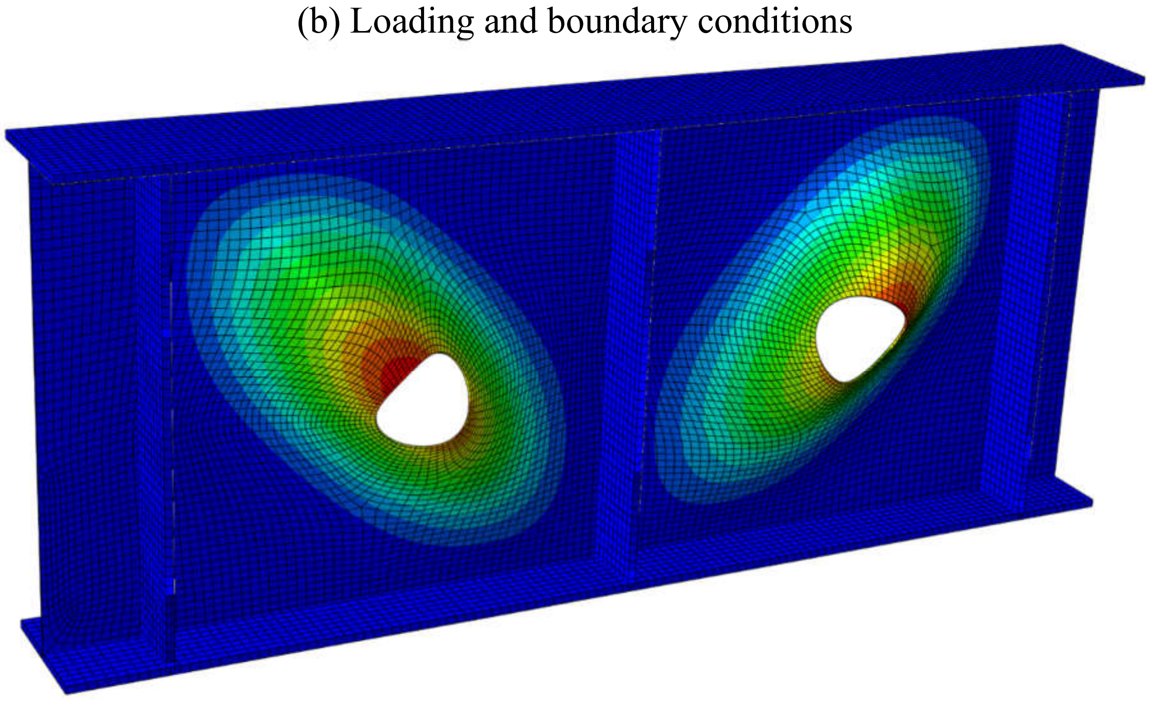

(c) Buckling analysis

**Fig. 12. Development of numerical models**

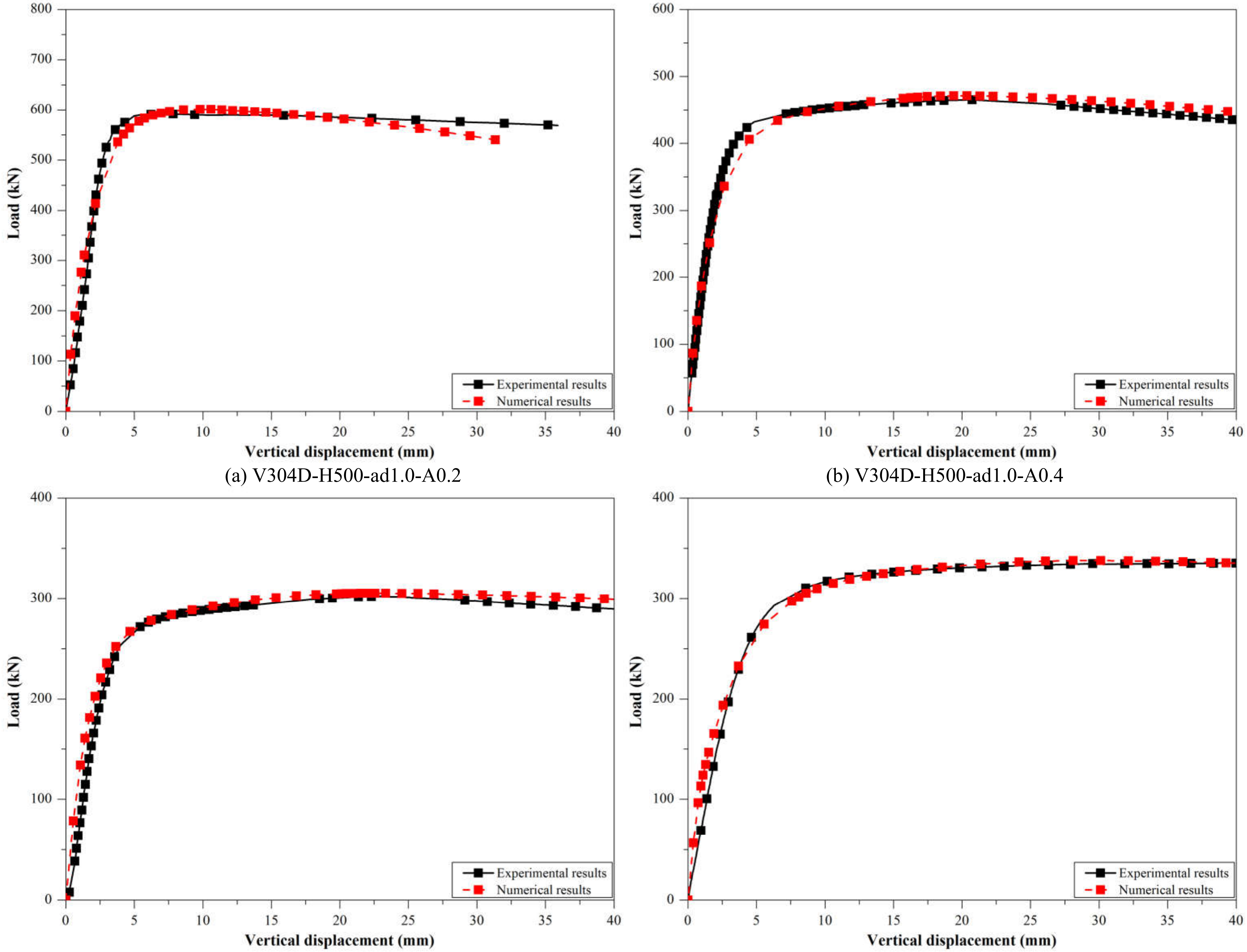


(a) V304D-H500-ad1.0-A0.2

(b) V304D-H500-ad1.0-A0.4

(c) V304D-H500-ad1.0-A0.6

(d) V304D-H700-ad1.0-A0.6

**Fig. 13. Ultimate strength versus displacement relationship generated from the laboratory tests and numerical investigation**

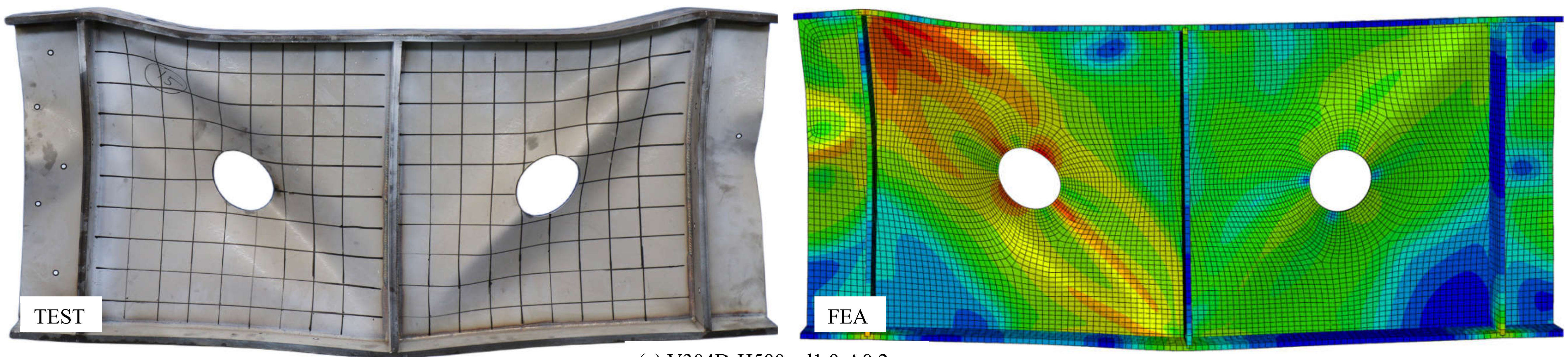


(a) V304D-H500-ad1.0-A0.2

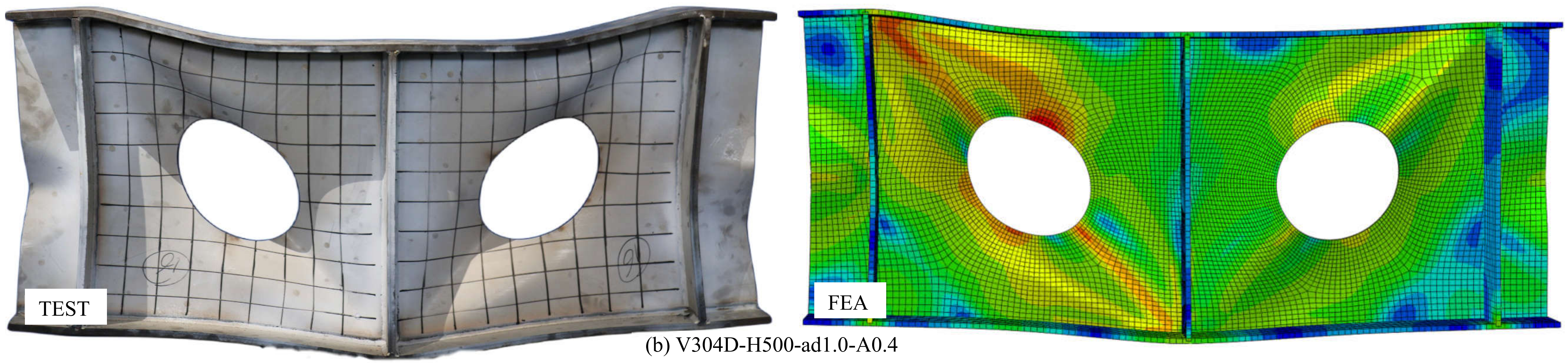


(b) V304D-H500-ad1.0-A0.4

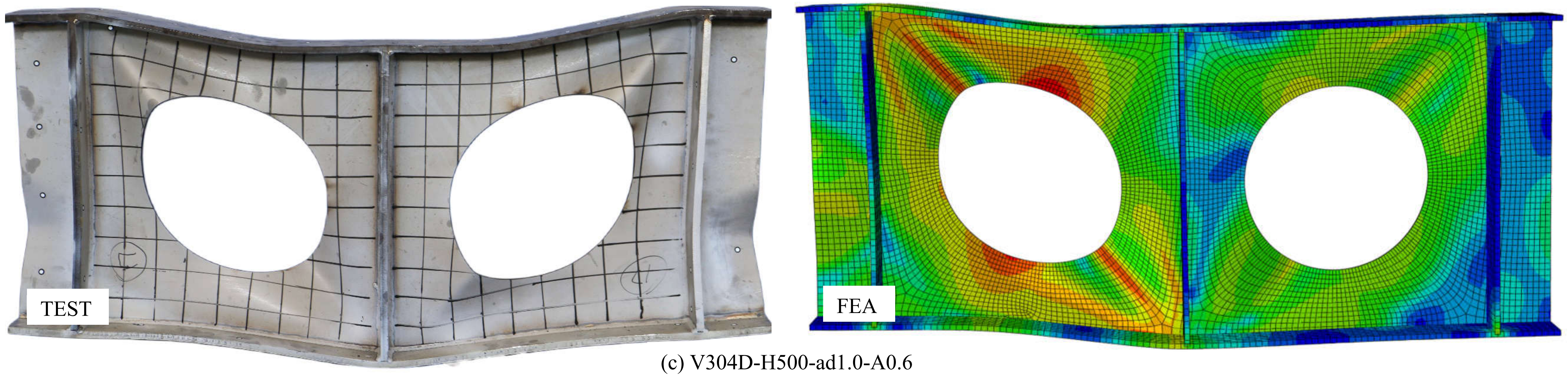


(c) V304D-H500-ad1.0-A0.6

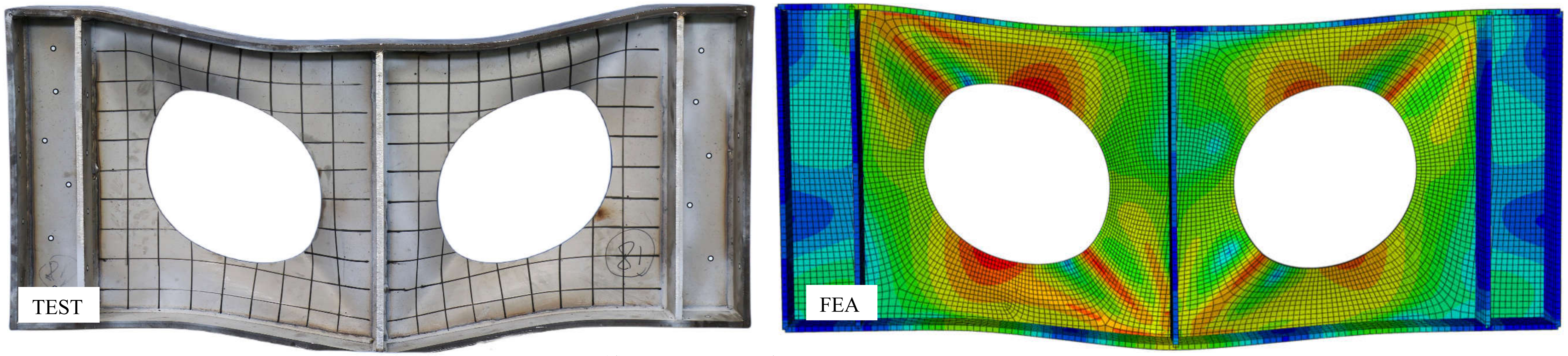


(d) V304D-H500-ad1.0-A0.6-R

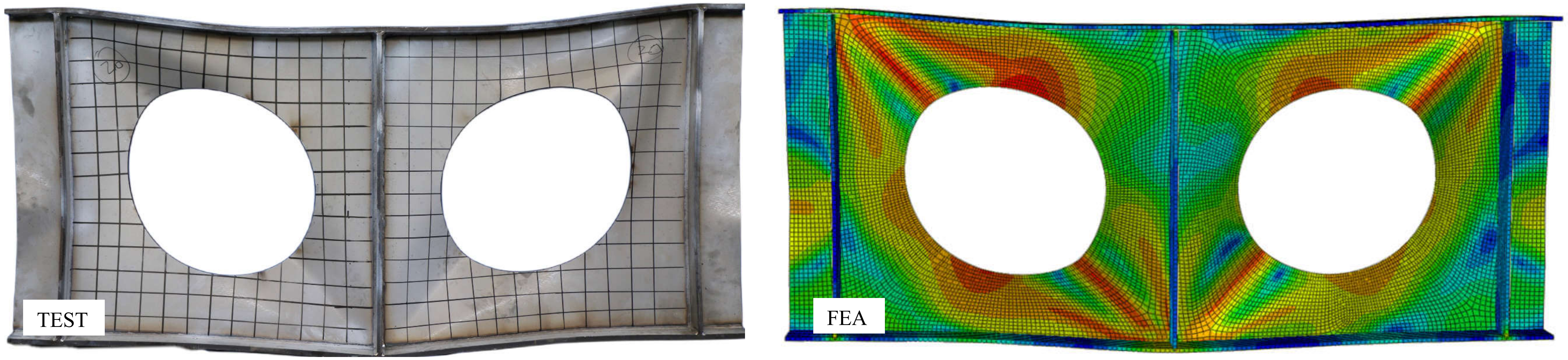


(e) V304D-H700-ad1.0-A0.6

**Fig. 14. Typical failure modes from the laboratory tests and numerical investigation**

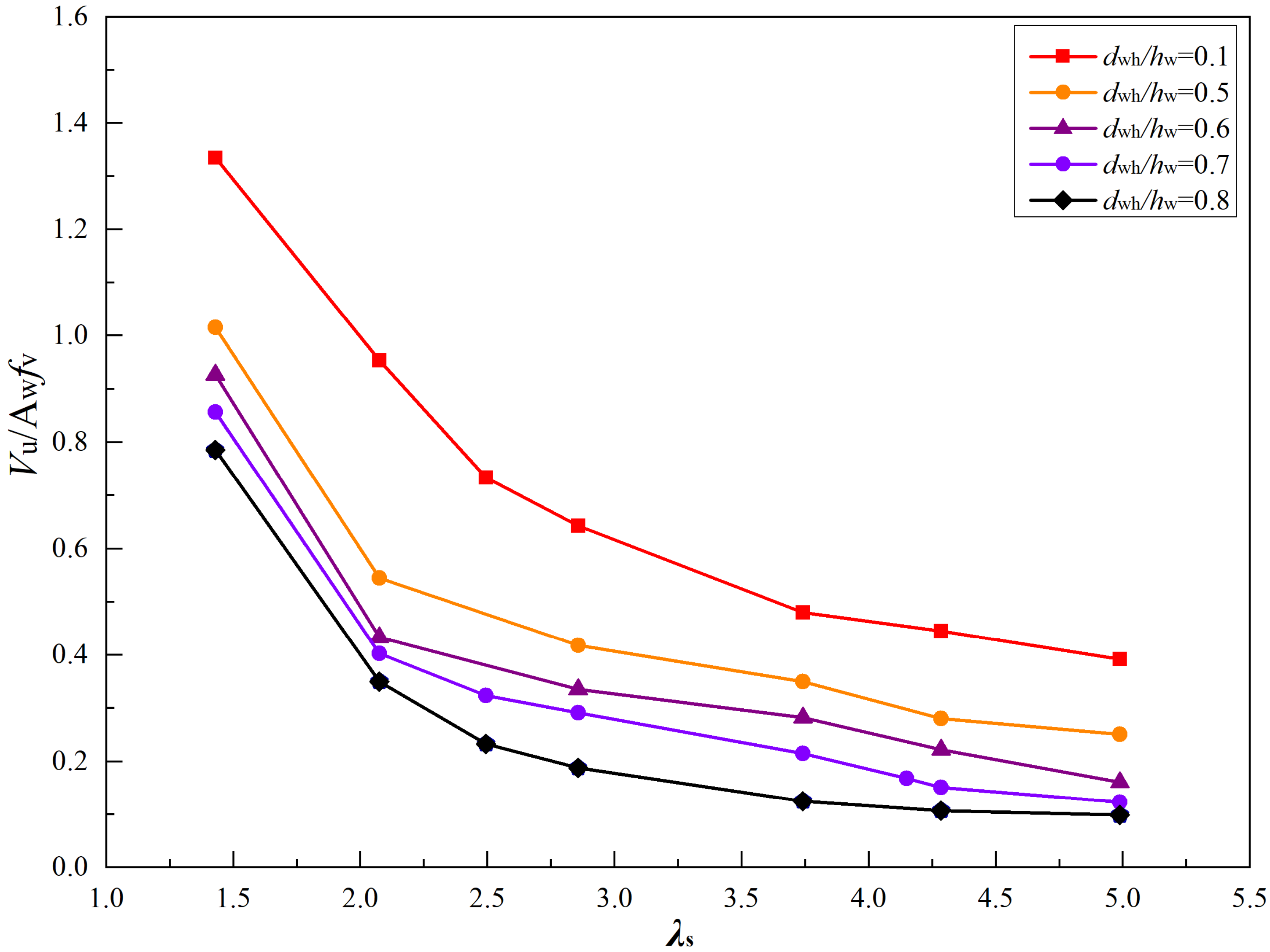


(a) Comparison of shear reduction factor between different hole ratios

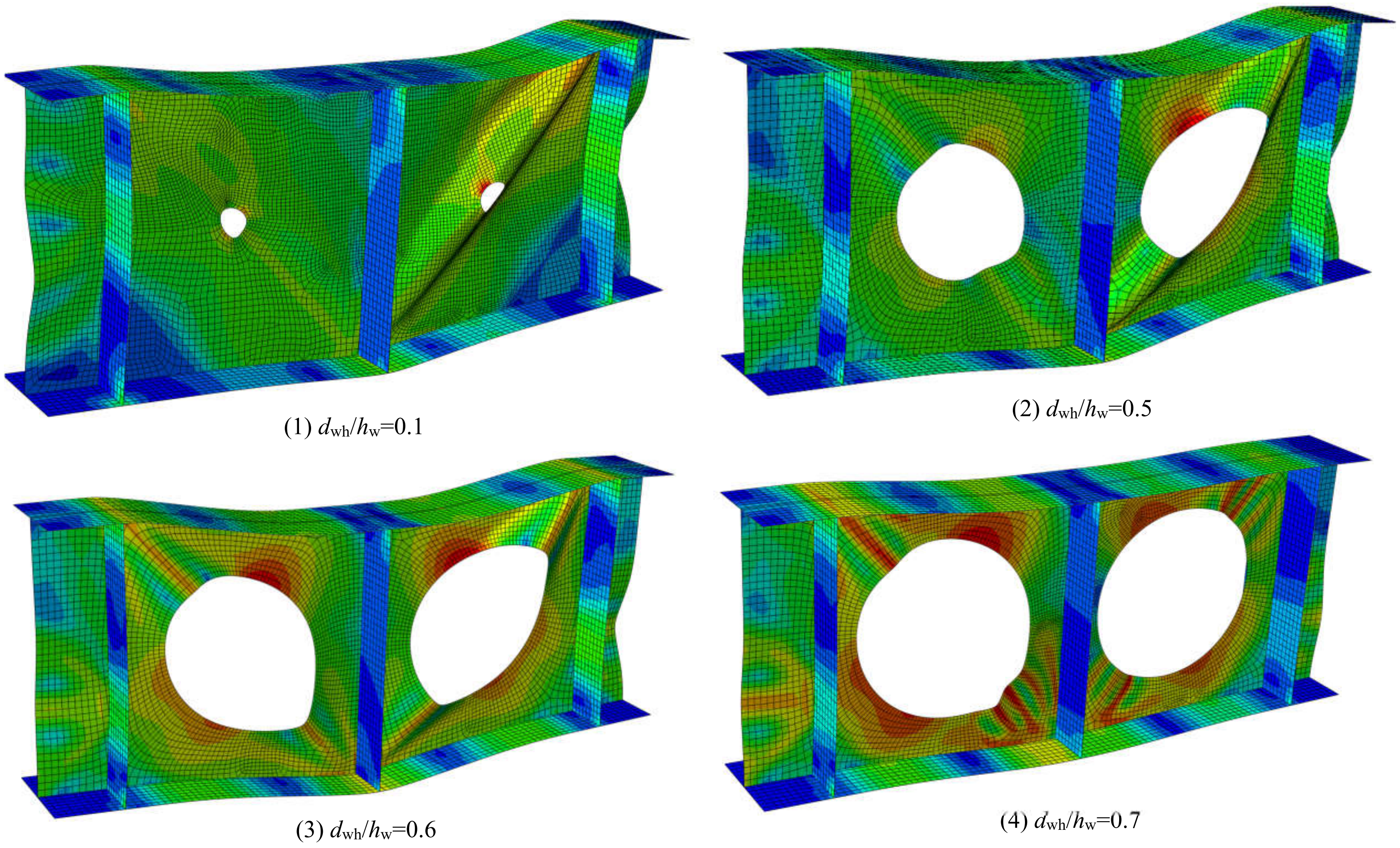

(1) $d_{wh}/h_w$=0.1

(2) $d_{wh}/h_w$=0.5

(3) $d_{wh}/h_w$=0.6

(4) $d_{wh}/h_w$=0.7

(b) Comparison of failure mode between different hole ratios

**Fig. 15. Effect of hole ratio on shear buckling behaviour**

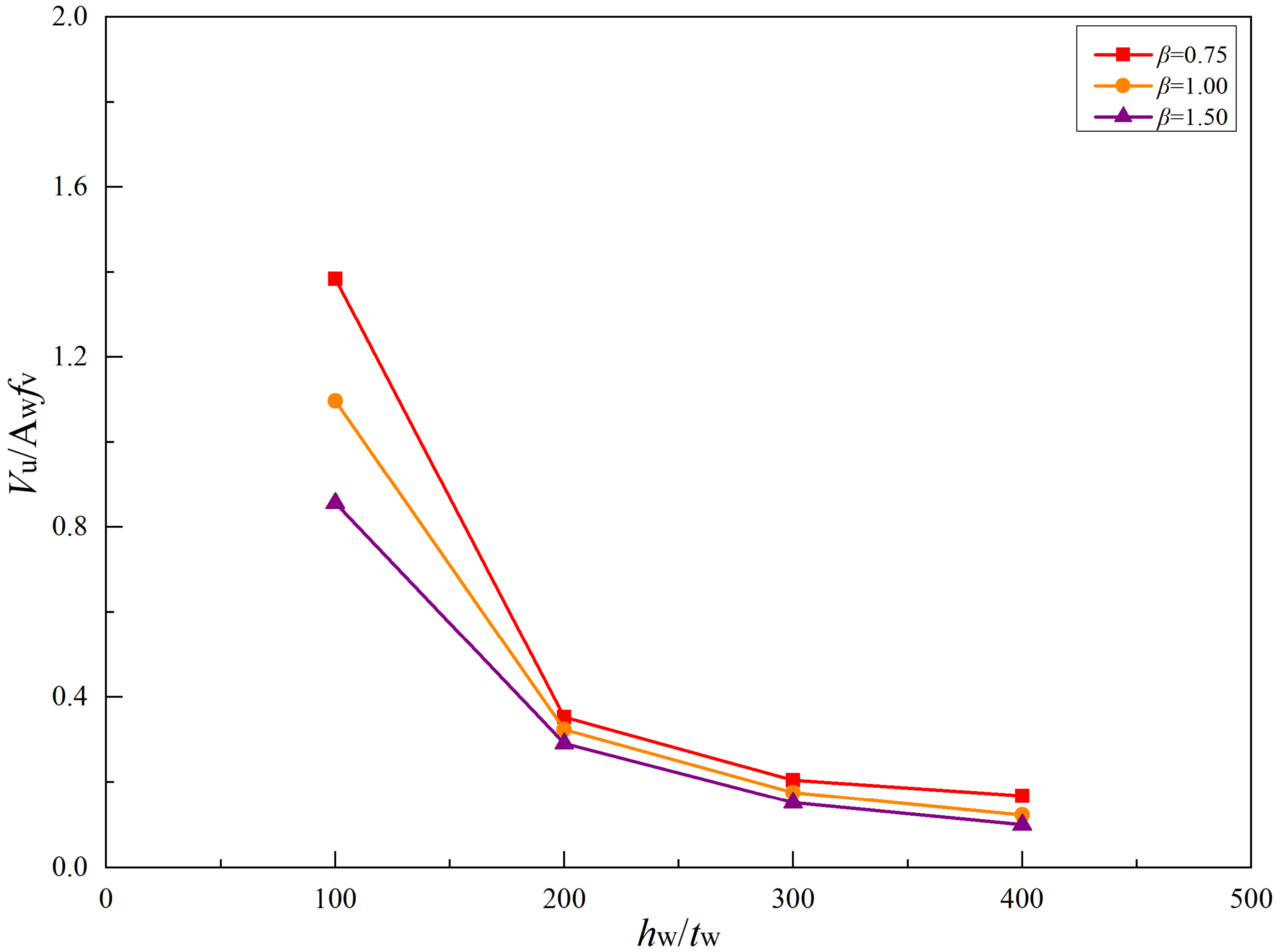


(a) Comparison of shear reduction factor between four different aspect ratios

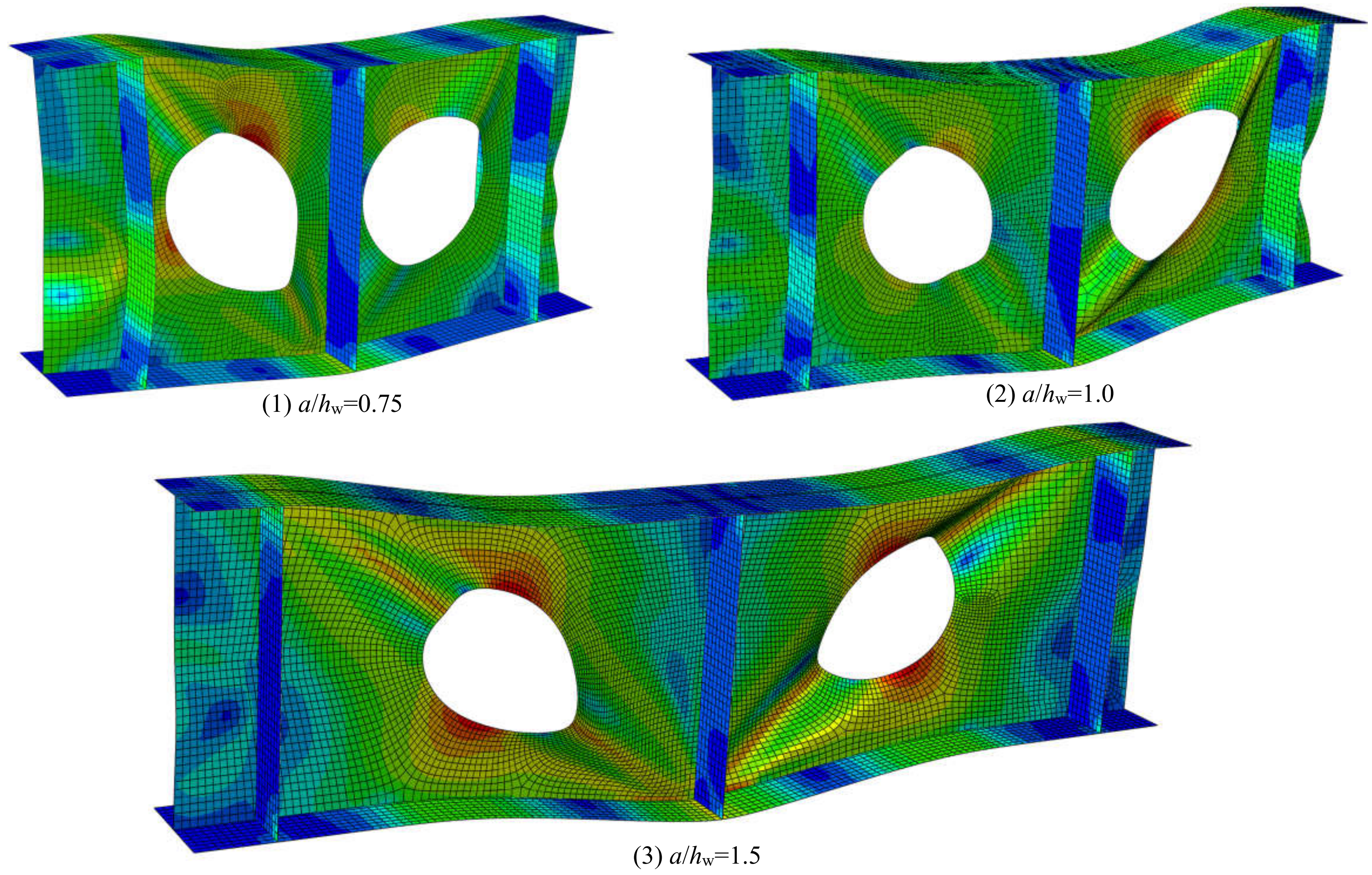


(b) Comparison of failure mode between four different aspect ratios

**Fig. 16. Effect of aspect ratio on shear buckling behaviour**

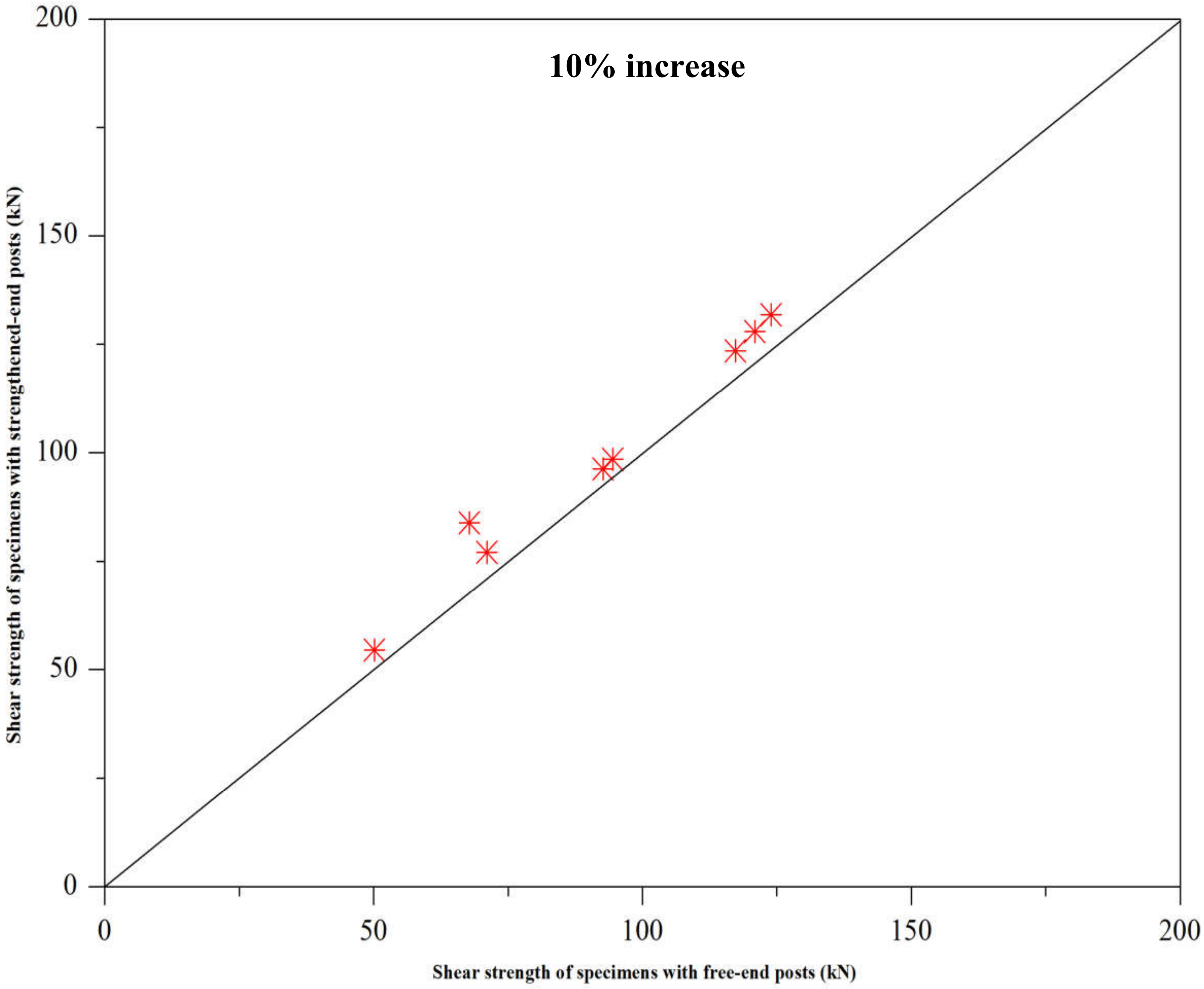


(a) Comparison of ultimate strength between two different end posts

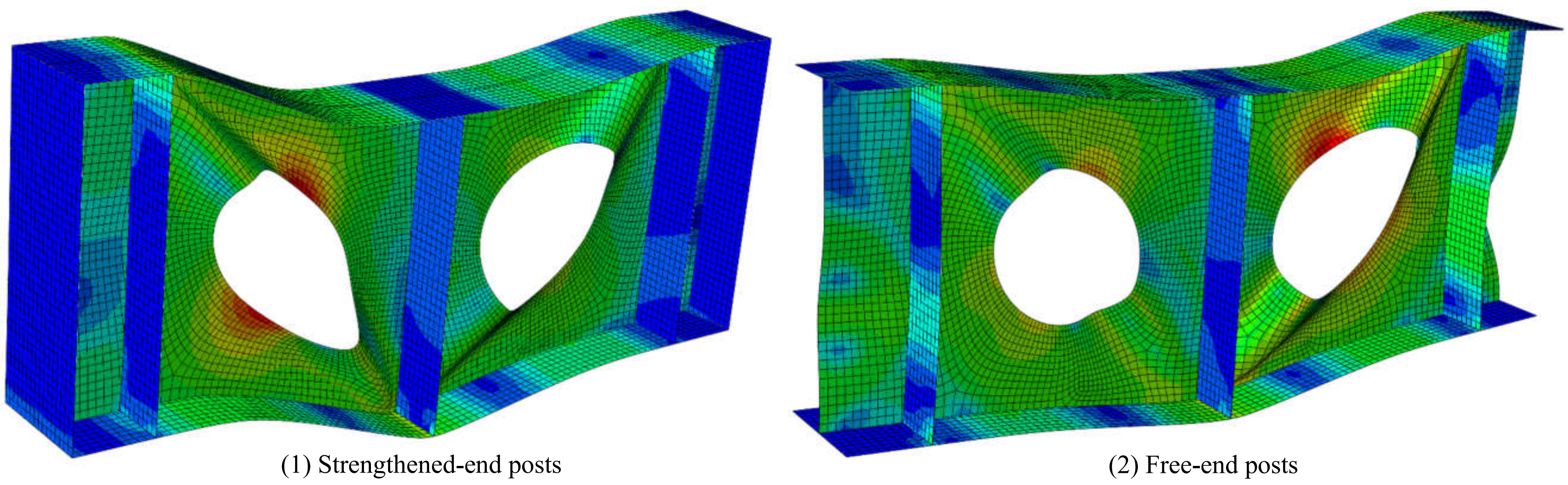

(1) Strengthened-end posts

(2) Free-end posts

(b) Comparison of failure mode between two different end posts

**Fig. 17. Effect of end posts on shear buckling behaviour**

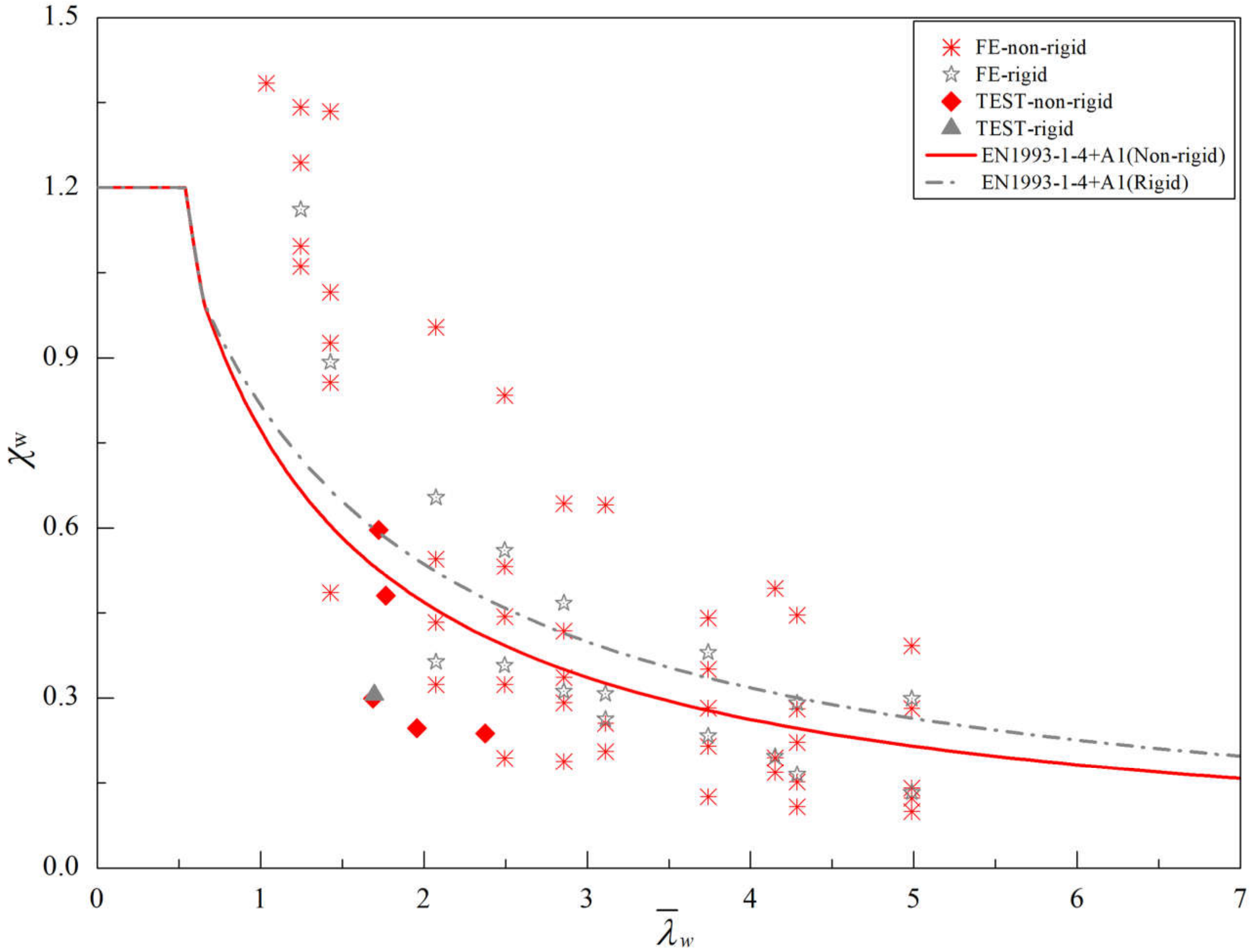


**Fig. 18. Comparison of test and FE results with the design curves of EN 1993-1-4+A1 [13]**

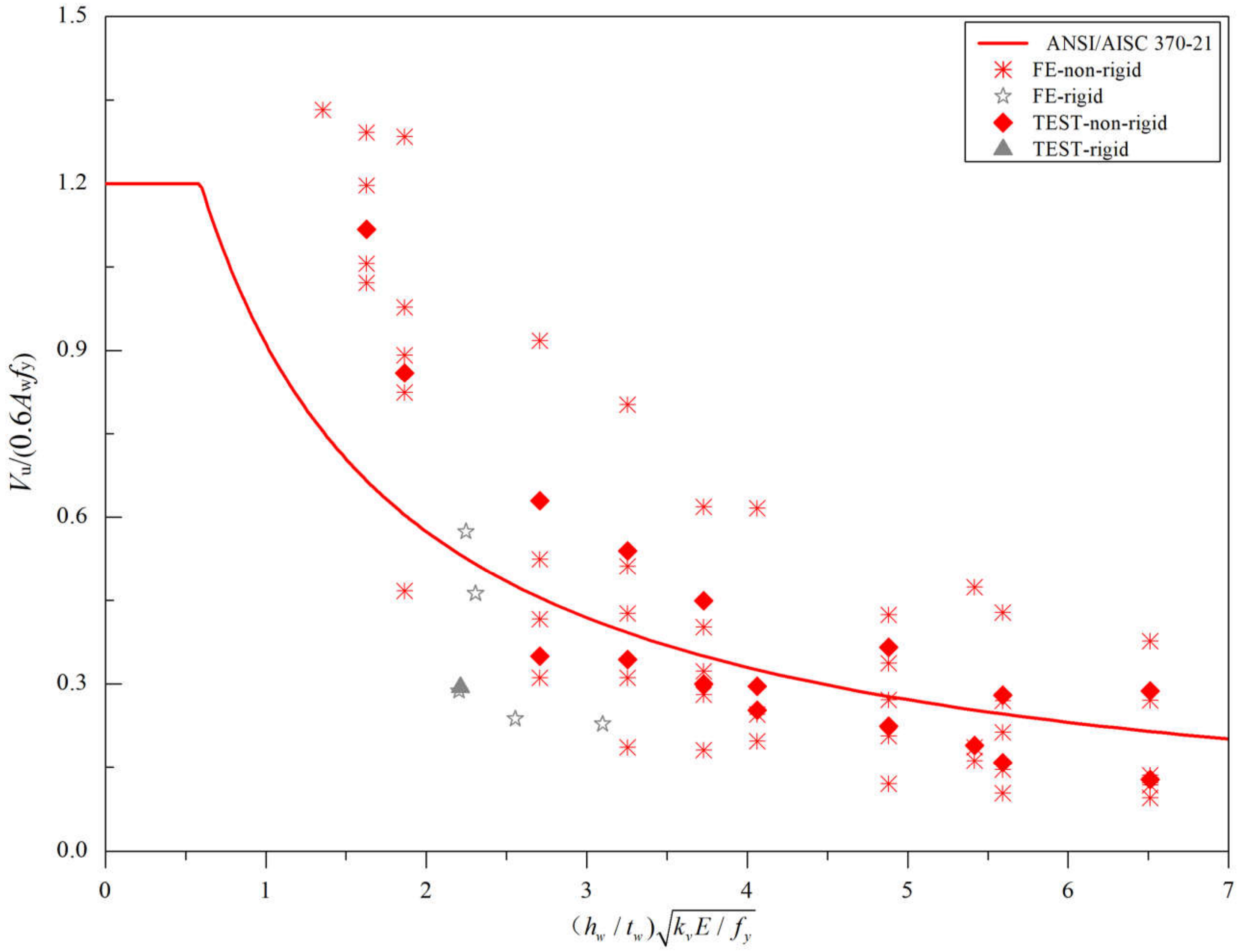


**Fig. 19. Comparison of test and FE results with the design curves of ANSI/AISC 370-21[14]**